

1 ~~Intensified~~ Sustained intensification of the Aleutian Low induces
2 weak tropical Pacific ~~Decadal Variability~~ sea surface warming

3
4 William J. Dow¹, Christine M. McKenna¹, Manoj M. Joshi², Adam T. Blaker³, Richard Rigby¹,
5 Amanda C. Maycock¹

6
7 ¹School of Earth and Environment, University of Leeds, Leeds, UK

8 ²Climatic Research Unit, School of Environmental Sciences, University of East Anglia, Norwich,
9 UK

10 ³National Oceanography Centre, Southampton, UK

11
12
13 [Correspondence: William J. Dow \(earwd@leeds.ac.uk\)](mailto:earwd@leeds.ac.uk)

14
15
16
17
18 **Abstract**

19
20 ~~The~~
21 ~~It has been proposed that externally forced trends in the~~ Aleutian Low ~~drives decadal variability in~~
22 ~~North Pacific sea surface temperatures (SST), but its role in basin-wide can induce a basin-wide~~
23 ~~Pacific SST variability is less clear owing to the difficulty of disentangling coupled atmosphere-~~
24 ~~ocean processes. We~~ response that projects onto the pattern of the Pacific Decadal Oscillation
25 (PDO). To investigate this hypothesis, we apply local atmospheric nudging in an intermediate
26 complexity climate model to isolate the effects of an ~~intense~~ intensified winter Aleutian Low ~~using~~
27 ~~an intermediate complexity climate model sustained over several decades.~~ An ~~intensified~~
28 intensification of the Aleutian Low produces a basin-wide SST response with a similar pattern to
29 ~~the model's internally-generated Pacific Decadal Oscillation (PDO).~~ PDO. The amplitude of the
30 SST response in the North Pacific is comparable to ~~the~~ PDO, but in the tropics and southern
31 subtropics the anomalies induced by the ~~intense~~ imposed Aleutian Low ~~anomaly~~ are a factor of 3
32 weaker than for the internally-generated PDO. The tropical Pacific warming peaks in boreal spring,
33 though anomalies persist year-round. A heat budget analysis shows the northern subtropical

34 Pacific SST response is predominantly driven by anomalous surface turbulent heat fluxes in boreal
35 winter, while in the equatorial Pacific the response is mainly due to meridional heat advection in
36 boreal spring. The propagation of anomalies from the extratropics to the tropics can be explained
37 by the seasonal footprinting mechanism, involving the wind-evaporation-SST feedback. The
38 results show that low frequency variability and trends in the Aleutian Low could contribute to basin-
39 wide anomalous Pacific SST, but the magnitude of the effect ~~cannot explain~~ the ~~full amplitude~~
40 ~~of tropical Pacific, even for~~ the ~~PDO~~. ~~This finding suggests that extreme Aleutian Low forcing~~
41 ~~applied here, is small. Therefore,~~ external forcing of the Aleutian Low is unlikely to ~~explain account~~
42 ~~for~~ observed ~~shifts~~ decadal SST trends in the ~~phase of PDO~~ tropical Pacific in the late 20th and
43 early-21st centuries.

44
45
46
47

48 Key points (140 chars)

49
50

Relaxing towards a strong

- 51 1. A sustained intensification of the winter Aleutian Low produces weak warming ~~across~~ in the
52 equatorial tropical Pacific that peaks in ~~boreal~~ spring.
- 53 2. Changes to surface heat fluxes (subtropics) during boreal winter and meridional advection
54 (equatorial) during boreal spring in the upper ocean drive the SST warming.
- 55 3. A combination of the seasonal footprint mechanism and wind-evaporation-SST mechanism
56 generate the surface climate anomalies in the tropical Pacific.

57
58
59
60

|

| 61
| 62
| 63
| 64

65 1. Introduction

66 _____
67 _____
68 The Aleutian Low has a well-known role in determining the North Pacific component of the Pacific
69 Decadal Oscillation (PDO) (e.g. Schneider and Cornuelle, 2005; Zhang et al., 2018; Hu and Guan,
70 2018; Sun and Wang, 2006; Newman et al. 2016). Fluctuations in ~~the~~ Aleutian Low intensity affect
71 the North Pacific subpolar gyre (Pickart et al. 2008), upper ocean temperatures (e.g. Latif and
72 Barnett, 1996) and sea surface height (Nagano and Wakita, 2019) through anomalous thermal
73 forcing and wind stress. Oceanic Rossby waves initiated by Aleutian Low variability can propagate
74 westward and cause lagged signals in the Kuroshio-Oshashio Extension (KOE) region (e.g., Kwon
75 and Deser, 2007).

76
77 The ~~prevailing traditional~~ paradigm for the PDO ~~regards describes~~ the ~~role integrated effect~~ of ~~the~~
78 ~~Aleutian Low to be largely driven by mid-latitude stochastic variability, which induces SST~~
79 ~~anomalies through turbulent heat flux and wind stress curl anomalies, and driving from~~ tropical
80 processes (~~ENSO variability~~) via excitation of ~~upper tropospheric~~-Rossby ~~waves wave trains and~~
81 ~~tropical-extratropical teleconnections~~ (Newman et al. 2016; Zhao et al. 2021; Vimont. 2005;
82 Knutson and Manabe 1998; Jin 2001). ~~We note that recent definitions separate low frequency~~
83 ~~PDO variability and show this is predominantly associated with stochastic extratropical~~
84 ~~atmospheric variability (i.e. the Aleutian Low) (Wills et al., 2018, 2019).~~ However, decadal changes
85 in the Aleutian Low may arise via other mechanisms including Arctic sea ice trends (Simon et al.
86 2021; Deser et al. 2016), ~~Arctic~~-stratospheric polar vortex variability (Richter et al., 2015), or as a
87 local response to external forcings (Smith et al. 2016; Dow et al. 2021; Dittus et al. 2021; Klavans
88 et al. submitted). It has been proposed that observed shifts in the PDO in the late 20th and early
89 21st centuries were driven by anthropogenic forcing of the Aleutian Low, which was then
90 communicated to a basin-wide PDO signal (Smith et al. 2016; Klavans et al. submitted; Gan et al.
91 2017). However, the mechanisms by via which North Pacific anomalies linked to decadal Aleutian
92 Low changes may be communicated into a basin-wide SST response including the tropics, and
93 whether the amplitude of such a response matches observed variations, remain unclear.

94
95 ~~Several studies have investigated the North Pacific influence on the tropics using surface flux~~
96 ~~restoring in a model (Alexander et al. 2010; Sun and Okumura 2019; Liu et al. 2021). Alexander~~
97 ~~et al. (2010) and Sun and Okumura (2019) imposed surface flux anomalies derived from the North~~
98 ~~Pacific Oscillation (NPO) the anomalous North Pacific pattern projecting onto the second EOF of~~

low frequency tropical Pacific SST variability. They showed that surface forcing associated with the NPO can affect decadal variability in the tropics. The proposed mechanism for communication of extratropical surface anomalies into the tropics is the seasonal footprinting mechanism (SFM) (Alexander et al. 2010; Sun and Okumura 2019; Amaya et al. 2019, Liu et al. 2021). Atmospheric circulation anomalies driven by the subtropical portion of the high latitude SST footprint modulate tropical SSTs through coupled atmosphere-ocean processes, leading to anomalies that persist through boreal spring-summer. However, the amplitude of the effect on tropical Pacific SSTs from the North Pacific has been suggested to be quite weak on decadal timescales (Alexander et al. 2010; Sun and Okumura 2019; Liguori and Di Lorenzo 2019). Moreover, the studies did not directly isolate driving by the Aleutian Low, which has been highlighted in studies arguing a role for anthropogenic forcing of recent observed PDO variability (Smith et al. 2016; Klavans et al. submitted).

In this study, we aim to better understand the role of long-term changes in the Aleutian Low in governing the multi-annual behaviour of tropical Pacific SSTs. We perform an ensemble of atmospheric nudging simulations in an intermediate complexity coupled climate model to isolate the effect of an anomalous sustained anomaly in the Aleutian Low and compare. The response to this with regional perturbation is compared to the internally-generated low frequency Pacific variability in a free running simulation. The manuscript is structured as follows: section 2 describes the methodology and details of the model used. Section 3 compares the results of the nudging simulations with the free running simulation. Discussion of the results is provided in section 4 and conclusions in section 5.

2. Data and Methods

2.1 FORTE 2.0

Simulations were performed using FORTE2.0, an intermediate complexity coupled Atmosphere-Ocean-Atmosphere-Ocean General Circulation Model (AOGCM) (Blaker et al., 2021). The atmospheric model IGCM4 (Intermediate General Circulation Model 4) (Joshi et al., 2015) uses a truncated series of spherical harmonics run at T42 resolution with 20 Σ -levels to a height of $\Sigma = 0.05$. IGCM4 is coupled to the MOMA (Modular Ocean Model – Array) (Webb, 1996) ocean model run at $2^\circ \times 2^\circ$ resolution with 15 vertical levels. The two components are coupled once per

135 day using OASIS version 2.3 (Terray et al., 1999) and PVM version 3.4.6 (Parallel Virtual
 136 Machine). As described in Blaker et al. (2021), between 5° N/S and the equator the horizontal
 137 ocean diffusion increases by a factor of 20 to balance equatorial upwelling and parameterise the
 138 eddy heat convergence. For more details on the model see Blaker et al. (2021). The model
 139 simulates ~~low-frequency multi-decadal~~ SST variability in the Pacific with a similar pattern to that
 140 seen in observations but a weaker amplitude by around a factor of 4 to 5 (Figure S1). While the
 141 model is run at relatively low horizontal and vertical resolution, the model code is sufficiently
 142 flexible to apply the nudging method described in Section 2,2 and the model is computationally
 143 efficient to run enabling a large ensemble to be produced.

146 2.2 Grid-point nudging method

148 Atmospheric nudging has been used to investigate climate and weather relationships between
 149 remote phenomena (e.g. Martin et al., 2021; Knight et al., 2017; Watson et al., 2016). A nudging
 150 code was added to IGCM4. Nudging was performed by adding tendencies to horizontal winds,
 151 temperature and surface pressure. The nudging code is publicly available at
 152 ~~(<https://github.com/NOC-MSM/FORTE2.0>~~~~<https://github.com/NOC-MSM/FORTE2.0>~~).

153 The nudging configuration is similar to that in Watson et al. (2016), with two additional terms to
 154 account for vertical (z) and temporal (t) variation in the nudging strength:

~~$$\delta x(\lambda, \phi, z, t) = -\gamma(\lambda, \phi, z, t)(x(\lambda, \phi, z, t) - x_{ref}(\lambda, \phi, z, t))/\tau, \quad (\text{Eqn 1})$$~~

~~$$\delta x(\lambda, \phi, z, t) = -\gamma(\lambda, \phi)g(z)h(t)(x(\lambda, \phi, z, t) - x_{ref}(\lambda, \phi, z, t))/\tau, \quad (\text{Eqn 1})$$~~

157 (Eqn 1)

158 where ~~x~~ is the variable being relaxed as a function of longitude (~~λ~~) and latitude (ϕ), x_{ref} is the reference state, and τ is the nudging
 159 strength (set to 6hr). The spatial extent of the nudging was tested extensively to avoid any shock
 160 at the boundaries and spurious effects of nudging near polar regions. The regional extent was
 161 determined as:

~~$$\gamma(\phi, \lambda) = f(\phi, \phi_1, \phi_2)f(\lambda, \lambda_1, \lambda_2), \quad (\text{Eqn 2})$$~~

~~$$\gamma(\phi, \lambda) = ff_1(\phi, \phi_1, \phi_2)ff_2(\lambda, \lambda_1, \lambda_2), \quad (\text{Eqn 2})$$~~

165 where

$$166 \quad f(\phi, \phi_1, \phi_2) = [1/(1 + e^{-(\phi - \phi_1)/\delta_1})][1 - 1/(1 + e^{-(\phi - \phi_2)/\delta_2})] f_1(\phi, \phi_1, \phi_2) = [1/(1 + e^{-(\phi - \phi_1)/\delta_1})][1 - 1/(1 + e^{-(\phi - \phi_2)/\delta_2})] \quad (\text{Eqn 3})$$

168 and

$$169 \quad f(\lambda, \lambda_1, \lambda_2) = [1/(1 + e^{-(\lambda - \lambda_1)/\delta_{31}})][1 - 1/(1 + e^{-(\lambda - \lambda_2)/\delta_{32}})] \quad (\text{Eqn 4})$$

$$170 \quad f_2 f(\lambda, \lambda_1, \lambda_2) = [1/(1 + e^{-(\lambda - \lambda_1)/\delta_{31}})][1 - 1/(1 + e^{-(\lambda - \lambda_2)/\delta_{32}})] \quad (\text{Eqn 4})$$

171

172 $\Phi_1 = 30^\circ\text{N}$ and $\Phi_2 = 65^\circ\text{N}$ represent the southern and northern limits-nodal points of the nudging
173 region and $\lambda_1 = 160^\circ\text{E}$ and $\lambda_2 = 140^\circ\text{W}$ are the western and eastern limits-nodal points of the
174 nudging region. The coefficients $\delta_1 = 0.05$, $\delta_2 = 1$, $\delta_3 = 0.2$. The horizontal limits follow the
175 commonly defined North Pacific Index (NPI) (Trenberth and Hurrell, 1994) as a proxy for the region
176 encompassed by the Aleutian Low. Within the nudging patch shown in Fig. S2, the values are
177 scaled so that the maximum value equals 1.

178 The temporal and nudging variations are determined as:

$$179 \quad g(z) = a \cdot \exp(-bz) \quad (\text{Eqn 5})$$

$$180 \quad h(t) = \exp\left(\frac{-d^2}{(2b^2)^2\mu}\right) \quad (\text{Eqn 6})$$

181 The strength of the tropospheric nudging is set to 1 (constant a, Equation 5) at $z_{\Sigma} = 0.96$ (lowest
182 atmospheric level), decreasing exponentially to 0 at $z_{\Sigma} = 0.05$ (tropopause) (Equation 5). Nudging
183 is applied during the extended boreal winter season (NDJFM) peaking on 15 January, with a
184 Gaussian function in time to increase the nudging strength from 0 to 1 between 1 to 30 November
185 and a reverse ramp-down during March. Term d (Equation 6) is the time difference relative to
186 maximum nudging time in months (e.g. d = 0 on 15th Dec, d = -1 on 15th Jan, etc.), β is a constant
187 set to 1.2, μ is a constant set to 2. Outside of the nudging window, $h = 0$. The spatio-temporal
188 forms of the nudging coefficients are shown in Figure S2.

189

190 The strong Aleutian Low state is taken from a 100 year long control run (CONTROL) based on a
191 winter month with an NPI anomaly of -3.02σ , -10.76 hPa, or -3.02σ , where $\sigma = 3.53$ hPa is the

192 standard deviation calculated over all winter months in CONTROL- (Figure S3). Therefore, the
 193 target state represents an extreme intense Aleutian Low state as simulated in FORTE2.0.
 194 ~~Comparing with ERA5 reanalysis data from 1979-2020, a 1σ NPI anomaly is 5.20 hPa. The~~
 195 ~~imposed atmospheric forcing is therefore weaker than if an equivalent experiment was conducted~~
 196 ~~using a comparably sized NPI anomaly in reanalysis data comprises the anomaly of this month~~
 197 ~~added to the daily climatology.~~ A 50 member NUDGED ensemble was generated using initial
 198 conditions drawn from each January 1st of the final 50 years of CONTROL. Each member is
 199 integrated for 30 years with nudging commencing on 1 November of the first year and repeating
 200 each winter of the simulation. Unless otherwise stated, the analysis shows ensemble mean
 201 anomalies in the NUDGED simulation compared to the long-term climatology of CONTROL.
 202 Statistical significance of the ensemble mean difference is ~~defined~~ estimated by comparing the
 203 ~~responses to the magnitude of internal variability. For CONTROL, variability is calculated by~~
 204 ~~multiplying the standard deviation of overlapping 15-year means by $\sqrt{2}$.~~

205 ~~The median value of the standard deviation is used and the result is statistically significant at the~~
 206 ~~95% level if the ensemble mean response lies outside of the bounds $\pm 1.96 \times \text{SD}$.~~
 207 where the ensemble mean response lies more than as being where the anomaly ± 2 standard
 208 errors does not overlap zero. Standard error (SE) is calculated as

$$\text{SE} = \sigma / \sqrt{n} \quad (\text{Eqn. 7})$$

210 Where σ is the inter-ensemble standard deviation of the time averaged anomaly of interest and n
 211 is the ensemble size defined by the spread of the, 50-ensemble member responses, from
 212 CONTROL.

213 **2.3 Mixed Layer Heat Budget Analysis**

214 The heat budget of the upper 30m of the ocean (representing the mixed layer ~~(assumed to be 30~~
 215 ~~m deep)~~ is analysed for the regions shown by the boxes in Figure 1, where the temperature
 216 tendency is given by: ~~$dT/dt = \text{ADV} + \text{DIFF}_{\text{vert}} + \text{DIFF}_{\text{horiz}} + \text{CONV}$ (Eqn. 5).~~

$$dT/dt = \text{ADV} + \text{DIFF}_{\text{vert}} + \text{DIFF}_{\text{horiz}} + \text{CONV} \quad (\text{Eqn. 8})$$

218 Daily tendencies due to advection (ADV), vertical and horizontal diffusion ($\text{DIFF}_{\text{vert}}$ and $\text{DIFF}_{\text{horiz}}$)
 219 and convection (CONV) are output from the model. Further granularity in the heat budget terms
 220 (e.g. turbulent fluxes) was not possible due to the limited availability of diagnostics from the

221 model. Vertical diffusion represents the contribution to the mixed layer heat budget from surface
 222 turbulent and radiative fluxes. ADV is composed of zonal, meridional and vertical components:

$$223 \text{---} \frac{\delta T}{\delta x} \text{---} \frac{\delta T}{\delta y} \text{---} \frac{\delta T}{\delta z} \text{---}$$

$$224 \text{---} ADV = u \frac{\delta T}{\delta x} + v \frac{\delta T}{\delta y} + w \frac{\delta T}{\delta z} \text{---} \text{(Eqn. 6),}$$

$$225 \text{---} \text{---} \text{---}$$

$$226 \text{---} ADV = u \frac{\delta T}{\delta x} + v \frac{\delta T}{\delta y} + w \frac{\delta T}{\delta z} \text{---} \text{(Eqn. 98)}$$

227 where u, v and w are the zonal, meridional and vertical components of the ocean velocity and
 228 dT/dx represents the local zonal gradient of temperature. We linearize the meridional advection
 229 term to investigate the relative roles of changes to ocean current velocity and temperature gradient
 230 as follows:

$$231 \text{---} \frac{\delta T}{\delta y} \text{---} \frac{\delta T^0}{\delta y} \text{---} \frac{\delta T}{\delta y} \text{---} \frac{\delta T}{\delta y} \text{---}$$

$$232 \text{---} (v \frac{\delta T}{\delta y})' = v' \frac{\delta T^0}{\delta y} + v_0 (\frac{\delta T}{\delta y})' + v' (\frac{\delta T}{\delta y})' \text{---} \text{(Eqn. 7)}$$

$$233 \text{---} (v \frac{\delta T}{\delta y})' = v' \frac{\delta T^0}{\delta y} + v_0 (\frac{\delta T}{\delta y})' + v' (\frac{\delta T}{\delta y})' \text{---} \text{(Eqn. 109)}$$

234 where the subscript 0 denotes CONTROL values and primes denote anomalies in NUDGED.

235 2.4 PDO Index

236 The PDO index is calculated as the first EOF of monthly SST anomalies, calculated as deviations
 237 from the climatological seasonal cycle, over the region 20-65°N, 120-260°E- (Mantua et al. 1997).
 238 Before calculating the leading EOF, the temperature anomalies are weighted by the square-root
 239 of the cosine of latitude to account for the decrease in area towards the pole. The monthly principal
 240 component, corresponding to the PDO index, is normalised by the standard deviation to give it
 241 unit variance. The pattern of temperature anomalies that covaries with the PDO is found by linearly
 242 regressing the time series of the monthly mean temperature anomalies onto the monthly PDO
 243 index (Figure 1b). Here we define the PDO using the common index based on the leading EOF of
 244 North Pacific SST variability. Wills et al. (2019) showed that the tropical Pacific SST anomalies
 245 associated with this index are predominantly related to high frequency (e.g., ENSO) SST
 246 variability, while the extratropical part is related to turbulent heat flux and wind stress anomalies
 247 associated with intrinsic Aleutian Low variability. The discrepancy between the modelled and
 248 observed SST anomalies associated with the PDO index in Figure S1 could be due to the slightly
 249 weaker than observed ENSO amplitude in the model by around 33% (Figure S4) (see also Blaker
 250 et al., 2021).

251 **3. Results**

254 **3.1 Surface temperature response**

255 Figure 1a shows annual mean surface temperature anomalies in NUDGED expressed as a change
256 per standard deviation (σ) of the PDO index. Here, the anomaly between NUDGED and
257 CONTROL is projected onto the first EOF from the control run to generate a pseudo-PC. The
258 anomaly is divided by the pseudo-PC to calculate the anomaly per standard deviation of the PDO
259 index, expressed in a similar way to that derived from CONTROL. A horse-shoe pattern of
260 anomalous temperature extends across the North Pacific, comprising warming in the north and
261 eastern Pacific and along the west coast of North America and cooling in the western North
262 Pacific/KOE region. The strongest warming (0.2-0.3 K/ σ) is seen over the North Pacific and
263 western North America. There is weaker (0.02-0.04 K/ σ) but statistically significant warming in the
264 ~~eastern and central~~ equatorial Pacific. TheAcross the Pacific Ocean, the pattern of temperature
265 anomalies in NUDGED closely resembles unforced multidecadal Pacific variability in CONTROL
266 (Figure 1b-), with a pattern correlation coefficient of 0.53. Therefore, a sustained increase in
267 Aleutian Low strength forces a basin-wide SST response ~~that~~which resembles
268 ~~internally generated~~that associated with internally-generated coupled variability in CONTROL.
269 However, there are clear differences in the sign of the anomaly outside the North Pacific basin and
270 nudging region, such as over north-eastern Siberia and south-central USA. Furthermore, while the
271 extratropical SST anomalies are somewhat larger in NUDGED, particularly in the subpolar gyre,
272 the tropical Pacific signal is substantially weaker by a factor of ~ 3 . This indicates that atmospheric
273 forcing by the Aleutian Low alone is not sufficient to generate a basin-wide SST response that is
274 consistent with the intrinsic variability of the model. Note the Aleutian Low state in x_{ref} is extreme
275 (-3σ), meaning a more realistic amplitude for sustained Aleutian Low intensification can be
276 expected to induce a weaker response.

277 The seasonality of the surface temperature anomalies in NUDGED is shown in Figure 2 separated
278 for years 1-2, years 3-4 and years 5-30. The initial response to the intensified Aleutian Low is a
279 warming in the subpolar gyre in boreal autumn (SON). This amplifies in DJF during the peak of
280 the nudging period, where a tongue of warming extends into the subtropical North Pacific. This
281 pattern persists into MAM after nudging ceases but is also accompanied by warming in the eastern
282 tropical Pacific. By JJA, the tropical and subtropical temperature changes have weakened leaving
283 residual warming in the subpolar gyre that persists into the following winter. The temperature

284 anomalies over land quickly dissipate due to the low specific heat capacity. A similar seasonal
285 evolution occurs in years 3-4, but the tropical warm anomaly emerges earlier in DJF and extends
286 further westward at its peak in MAM. The anomalies in years 5-30 show a similar spatiotemporal
287 pattern to the first 4 years, suggesting the mechanisms by which the anomalies manifest do not
288 evolve strongly when the signals are maintained over multi-year timescales. Small differences
289 between years 1-4 and 5-30 are the extent of the robust signal in the tropical Pacific; there is a
290 small reduction in the amplitude of the tropical warming in JJA and no significant western tropical
291 Pacific warming in MAM for years 5-30. The signal of peak tropical warming in MAM in NUDGED
292 qualitatively agrees with observed low frequency Pacific variability (Figure S1), though we note
293 that FORTE2.0 shows a narrower band of tropical warming compared to observations.
294 Furthermore, the weak (up to ~10x weaker) footprint of modelled PDO variability in the equatorial
295 Pacific (Fig. S1) is consistent with a notion that Aleutian Low driven SST variability in the extra-
296 tropics has little influence on tropical variability (Wills et al., 2019; Zhao et 2021).

297

298

299 3.2 Mixed layer heat budget

300 The mixed layer heat budget in the subtropical North Pacific and Niño 3.4 regions shows different
301 annual cycles in the anomalous temperature tendencies (Figure 3 a,b). The largest anomalous
302 surface temperature tendency in the subtropical North Pacific occurs during the nudging period
303 (DJF), whereas the peak warming tendency in the Niño3.4 region occurs in February-April. In the
304 subtropics in winter, warming from vertical diffusion is offset by meridional advection. In contrast
305 in the Niño 3.4 region, anomalous meridional advection contributes to a warming tendency
306 year-round/year-round, with the maximum (~0.3 K/month) in MAM. This warming is partly offset by
307 anomalous vertical diffusion and convection. Meridional advection therefore contributes to cooling
308 in the subtropical North Pacific but causes warming in the Niño 3.4 region.

309

310 The anomalous meridional advection in the subtropical North Pacific is dominated by the change
311 in meridional velocity, whilst in the Niño3.4 region the change in meridional temperature gradient
312 is the largest contributor throughout most of the year (apart from Sept-Dec) (Figure 3 c,d). The
313 enhanced warming tendency from Feb-June in the Niño3.4 region is driven by changes in
314 meridional velocity. The difference in contributing terms implies different mechanisms governing
315 the changing mixed layer temperatures in the two regions.

316

317 The net surface heat flux anomalies in NUDGED are shown in Figure 4(a-d). There are positive
318 ~~(downward)~~ net surface heat flux anomalies across the North Pacific and within a SW-NE oriented
319 band in the subtropical North Pacific. The largest heat flux anomalies occur during DJF, with values
320 in excess of $4 \text{ W m}^{-2}/\sigma$. The net surface heat flux anomalies in NUDGED are dominated by the
321 latent heat flux (Fig. 4 e-h). The pattern of surface latent heat flux anomalies in JJA in the
322 extratropical North Pacific ~~resembles the SST pattern associated with the internal PDO (Fig. S1d)~~
323 ~~and represents a damping of the SST anomalies; positive flux anomalies extend eastward from~~
324 ~~the KOE region, which are enveloped by negative anomalies in the northeast Pacific and~~
325 ~~subtropical North Pacific, that for the internal PDO structure (Figure S3), with positive flux~~
326 ~~anomalies extending eastward from the KOE region, which are enveloped by negative anomalies~~
327 ~~in the northeast Pacific and subtropical North Pacific. The~~ The positive heat fluxes exhibited in the
328 KOE region in all seasons outside of DJF are evidence that cold SST anomalies in this region
329 reduce heat loss to the atmosphere throughout the simulations. Regions such as those in the
330 north-east North Pacific appear to dampen the SST anomalies during MAM and JJA, which may
331 indicate limited dynamic feedback to the atmosphere. However, across the central North Pacific,
332 the persistence of surface latent flux anomalies year-round is expected given the surface
333 temperature persistence and alludes to ~~oceanatmosphere~~ ocean-atmosphere feedbacks.

334

335

336 3.3 Atmospheric circulation response

337 Figure 5 shows the seasonal mean zonal and meridional near-surface wind anomalies in
338 NUDGED. As expected, the largest anomalies occur in the period over which nudging is applied
339 (DJF), with a westerly zonal wind anomaly of up to $\sim 0.5 \text{ ms}^{-1}/\sigma$ in the subtropics and an easterly
340 anomaly of a similar magnitude in the subpolar extratropics. The meridional wind shows alternating
341 southerly-northerly anomalies across the North Pacific orientated with a north-easterly tilt
342 suggesting ~~a Rossby wave train response that a persistently strong AL invokes a modulation of~~
343 ~~the climatological Rossby wave train providing a pathway for atmospheric communication between~~
344 ~~the North Pacific and eastern tropical Pacific. Evidence for the modulation of the Rossby wave~~
345 ~~train is further evident in the upper tropospheric winds (Figure S5). Recall that the nudging strength~~
346 ~~in the upper troposphere is several times weaker than at the surface (Fig. S2), so the upper-level~~
347 ~~circulation anomalies likely represent a response to the lower tropospheric forcing.~~ The subtropical

348 zonal wind anomalies ~~project onto~~represent a southerly shift of the westerlies compared to the
349 climatology in CONTROL, with persistent anomalies extending into the spring after nudging
350 ceases (April – not shown)(MAM). Interestingly, there is an emergence of a westerly wind anomaly
351 near the coast of CaliforniaCentral America in DJF that extends southward and westward into the
352 equatorial Pacific in MAM. Although zonal wind anomalies are evident in JJA, they are not strongly
353 statistically significant.

354 Figure 6 shows the latitude-time evolution of surface temperature, near-surface wind and surface
355 pressure anomalies in NUDGED averaged over the central and eastern tropical Pacific (which is
356 entirely outside the nudging region). There is year-round warming in subtropical and equatorial
357 regions, with the largest magnitude in the subtropics from November through April (~ 0.05 K/ σ) and
358 in the equatorial region from March through July (~ 0.3 K/ σ). The nudging invokes concurrent
359 warming in the subtropics, while there is a seasonal delay in the emergence of warming in the
360 equatorial Pacific. From July to November in the subtropics (around 15° N) there is substantially
361 less warming than during the rest of the year, with values close to zero. The westerly wind
362 anomalies coincide with the timing of the temperature anomalies, with south-westerly anomalies
363 of ~ 0.05 m s $^{-1}$ / σ in the subtropics and ~ 0.03 m s $^{-1}$ / σ in the equatorial region. In addition to the
364 cross-equatorial temperature gradient generated by the subtropical anomaly, the lower surface
365 pressure in the northern subtropics (~ 1.5 hPa), which is largest in February and March, creates a
366 pressure gradient across the equator-, a key component of the WES mechanism. At this time there
367 is evidence of cooling in the southern subtropics (south of 15° S).

368

369

370 **4. Discussion**

371

372 The impact of an intensified Aleutian Low on the tropical Pacific in this study suggests an excitation
373 of the SFM mechanism (e.g. Vimont et al. 2003; Alexander et al. 2010; Chen and Yu, 2020; Sun
374 and Okumura, 2019). In accordance with the SFM, the SST anomalies persist into the summer
375 season, with anomalous temperatures found in the North Pacific year-round. The signals in winter
376 and spring show a similar spatial signature to that found by Liguori and Di Lorenzo (2019), who
377 show an SST signature in the subtropics as a precursor to ENSO dynamics. Here we find a similar
378 effect on multi-year timescales in response to an anomalous Aleutian Low.

379

380 The midlatitude westerly winds show a southerly shift throughout the year which, in agreement
381 with Liu et al. (2021), acts to prevent heat loss from the surface in the northern subtropics due to
382 reduced evaporation. This in turn drives the SST anomaly towards the equator. Liu et al. (2021)
383 show the SFM as the mechanism that propagates SST anomalies southward, through a change
384 in latent heat fluxes. However, in DJF the westerly winds imposed by the nudging cause a
385 weakening of the subtropical trades; hence the southerly shift of westerlies starts to occur within
386 the season of nudging. We show anomalous latent heat flux is responsible for the change in
387 subtropical North Pacific SSTs. The limitation of the Liu et al. (2021) study is that the atmosphere
388 was coupled to a thermodynamic slab-ocean, whereas we integrate a fully coupled ocean model
389 allowing for a role of ocean dynamical feedbacks. Sun and Okumura (2019) conducted a related
390 investigation by imposing heat flux anomalies associated with the North Pacific Oscillation, (NPO)
391 which is a coupled atmosphere-ocean mode, but they imposed a fixed year round anomaly whereas
392 the Aleutian Low shows strongest variability in winter and therefore we only impose relaxation
393 during boreal winter in our experimental design. The simulations presented use an anomalous
394 Aleutian Low state taken from a single month (Figure S3). An area for future research is to impose
395 a suite of varying Aleutian Low states with different spatial and temporal profiles to test the
396 sensitivity of the responses described here to details of the imposed relaxation state.

397
398 In the tropical Pacific, the dominant mechanism responsible for the increase in SSTs is meridional
399 advection, with the change to meridional current velocity driving the accelerated warming in boreal
400 spring. This coincides with an anomalous northward cross-equatorial SST gradient and the
401 development of an anomalous cross-equatorial southward pressure gradient. Cross-equatorial
402 winds are generated, which, due to Coriolis force act to weaken the trades in the northern
403 equatorial region, decreasing the surface latent heat flux and leading to a local warming. The heat
404 budget analysis shows that surface heat fluxes are the primary warming agent during the nudging
405 period, whereas a change to surface advection drives the warming in the central tropical-near-
406 equatorial Pacific. A comprehensive review of this mechanism, commonly referred to as the wind-
407 evaporation-SST (WES) mechanism, is provided in Mahajan et al. (2008). Further, the mechanism
408 has been posited as a pathway through which North Pacific SSTs can influence ENSO variability
409 (Amaya et al. 2019). Investigation into The equatorial thermocline depth shows a slight deepening
410 of the thermocline in all seasons apart from SON, which is supported by changes in the vertical
411 advection term (not shown). Figure 7 gives a pictorial representation of the combined mechanisms
412 involved in translating the Aleutian Low anomaly into the deep tropics.

413

414 While the results make conceptual sense and are in broad agreement with studies using more
415 comprehensive modelling tools (see earlier references), the amplitude of the response could be
416 verified in other more detailed coupled climate models. The coarseness of the coupled model,
417 specifically the vertical dimension of the oceanic component, is a limitation of the study.
418 Furthermore, the model's relatively low resolution and inability to resolve mesoscale processes in
419 the ocean and atmosphere may affect the results of the study. Future studies using observations
420 and higher resolution GCMs to test the results herein would be valuable. Furthermore, to ensure
421 model stability, the anomalous nudging state was drawn from the coupled atmosphere-ocean
422 control simulation. The Aleutian Low variability sampled from this simulation therefore includes
423 effects from tropical variability. The month used as the reference state for the nudging coincides
424 with an ENSO state (magnitude = 0.55) in the tropical Pacific. Further study could investigate more
425 idealised AL states and their effects on extra-tropical-tropical communication.

428 **5. Conclusions**

430 Externally-forced Aleutian Low trends have been implicated as a potential driver of recent
431 variations in the Pacific Decadal Oscillation (Smith et al., 2016; Klavans et al., submitted). Here,
432 we have investigated the potential influence of Aleutian Low trends on basin-wide low frequency
433 Pacific sea surface temperature variability using nudging simulations in an intermediate complexity
434 climate model. The target Aleutian Low state represents an extremely intense Aleutian Low state
435 (-3σ of winter monthly variability) applied during boreal winter. The intensified Aleutian Low
436 induces a basin-wide SST response that resembles the model's internally-generated PDO with a
437 comparable amplitude in the extratropics, but a substantially weaker amplitude in the equatorial
438 Pacific by a factor of 4 to 5. The pattern of SST variability exhibited across the basin is evident on
439 interannual timescales as well as throughout the duration of the 30 year simulation.

441 The findings presented here support that the PDO can, at least in part, be driven by remotely
442 forced changes in the North Pacific atmospheric circulation independent of the tropics. However,
443 in our experiment the amplitude appears to be too weak to fully explain a multi-annual shift in the
444 PDO. across the tropics. This suggests that the hypothesis posed by Smith et al. (2016), ~~and~~
445 ~~Klavans et al. (submitted),~~ that anthropogenically forced changes in the Aleutian Low drove the
446 observed shift in the phase of the basin-wide PDO in the late 20th and early 21st centuries, should
447 be revisited.

448
449
450
451
452
453
454
455
456
457
458
459
460
461
462
463
464
465
466
467
468
469
470
471
472
473
474
475
476
477
478
479
480
481

Code availability

The nudging code used in the analysis can be found:
(~~<https://github.com/NOC-MSM/FORTE2.0>~~<https://github.com/NOC-MSM/FORTE2.0>).
).

Data availability

Underlying model data found in this paper is available from the corresponding author upon request.
~~HadISST data available: <https://www.metoffice.gov.uk/hadobs/hadisst/data/download.html>~~

~~HadISST data available: <https://www.metoffice.gov.uk/hadobs/hadisst/data/download.html>~~

Author contribution

WJD and ACM designed the study. WJD developed the nudging code in FORTE2.0 with support from CMM, MMJ and RR. ATB and RR helped with installation of FORTE2.0 at Leeds. WJD performed the analysis and produced the figures. WJD and ACM wrote the manuscript with comments from all authors. All simulations were performed on the ARC4 HPC at the University of Leeds.

Competing interests

The authors declare that they have no conflict of interest.

Acknowledgements

WJD was supported by a Natural Environment Research Council (NERC) Ph.D. studentship through the SPHERES Doctoral Training Partnership (NE/L002574/1) and by a Met Office

482 CASE studentship. ACM and CMM were supported by the European Union's Horizon 2020
483 Research and Innovation Programme under Grant Agreement 820829 (CONSTRAIN project).
484 ACM was supported by the Leverhulme Trust. We are grateful to Paloma Trascasa-Castro for
485 discussion of
486 ENSO processes. We are grateful for feedback on an earlier version of this manuscript from John
487 Marsham and Laura Wilcox.

488

489 **References**

490

491 Alexander, M. A., & Deser, C. (1995). A mechanism for the recurrence of wintertime
492 midlatitude SST anomalies. *Journal of Physical Oceanography*, 25(1), 122–137.
493 [https://doi.org/10.1175/1520-0485\(1995\)025<0122:AMFTRO>2.0.CO;2](https://doi.org/10.1175/1520-0485(1995)025<0122:AMFTRO>2.0.CO;2)

494 Alexander, M. A., Vimont, D. J., Chang, P., & Scott, J. D. (2010). The impact of extratropical
495 atmospheric variability on ENSO: Testing the seasonal footprinting mechanism using
496 coupled model experiments. *Journal of Climate*, 23(11), 2885–[2901](https://doi.org/10.1175/2010JCLI3205.1).
497 <https://doi.org/10.1175/2010JCLI3205.1>

498 ~~2901.~~ <https://doi.org/10.1175/2010JCLI3205.1>

499 Amaya, D. J., Kosaka, Y., Zhou, W., Zhang, Y., Xie, S. P., & Miller, A. J. (2019). The North
500 Pacific pacemaker effect on historical ENSO and its mechanisms. *Journal of Climate*,
501 32(22), 7643–7661. <https://doi.org/10.1175/JCLI-D-19-0040.1>

502 Barnett, T. P., Pierce, D. W., & Planck, M. (1999). Interdecadal interactions between the
503 tropics and midlatitudes in the Pacific basin. *Geophysical Research Letters*, 26(5),
504 615–618.

505 Blaker, A., Joshi, M., Sinha, B., Stevens, D., Smith, R., & Hirschi, J. (2021). FORTE 2.0: a
506 fast, parallel and flexible coupled climate model. *Geoscientific Model Development*,
507 [275–293](https://doi.org/10.5194/gmd-14-275-2021). <https://doi.org/10.5194/gmd-14-275-2021>

508 ~~275–293.~~ <https://doi.org/10.5194/gmd-14-275-2021>

509 Chen, S., & Yu, B. (2020). The seasonal footprinting mechanism in large ensemble
510 simulations of the second generation Canadian earth system model: uncertainty due to

511 internal climate variability. *Climate Dynamics*, 55(9–10), 2523–2541.
512 <https://doi.org/10.1007/s00382-020-05396-y>

513 Clement, A., DiNezio, P., & Deser, C. (2011). Rethinking the ocean's role in the Southern
514 Oscillation. *Journal of Climate*, 24(15), 4056–4072.
515 <https://doi.org/10.1175/2011JCLI3973.1>
516 <https://doi.org/10.1175/2011JCLI3973.1>

517 Czaja, A., van der Vaart, P., & Marshall, J. (2002). A diagnostic study of the role of remote
518 forcing in tropical Atlantic variability. *Journal of Climate*, 15(22), 3280–3290.
519 [https://doi.org/10.1175/1520-0442\(2002\)015<3280:ADSOTR>2.0.CO;2](https://doi.org/10.1175/1520-0442(2002)015<3280:ADSOTR>2.0.CO;2)
520 [https://doi.org/10.1175/1520-0442\(2002\)015<3280:ADSOTR>2.0.CO;2](https://doi.org/10.1175/1520-0442(2002)015<3280:ADSOTR>2.0.CO;2)

521 Deser, C., Sun, L., Tomas, R. A., & Screen, J. (2016). Does ocean coupling matter for the
522 northern extratropical response to projected Arctic sea ice loss? *Geophysical*
523 *Research Letters*, 43(5), 2149–2157. <https://doi.org/10.1002/2016GL067792>

524 Dittus, A. J., Hawkins, E., Robson, J. I., Smith, D. M., & Wilcox, L. J. (2021). Drivers of
525 Recent North Pacific Decadal Variability: The Role of Aerosol Forcing. *Earth's Future*,
526 9(12). <https://doi.org/10.1029/2021EF002249>

527 Dow, W. J., Maycock, A. C., Lofverstrom, M., & Smith, C. J. (2021). The effect of
528 anthropogenic aerosols on the aleutian low. *Journal of Climate*, 34(5), 1725–1741.
529 <https://doi.org/10.1175/JCLI-D-20-0423.1> <https://doi.org/10.1175/JCLI-D-20-0423.1>

530 [Gan, B. L. Wu, F Jia, S. Li, W. Cai, H. Nakamura, M. A. Alexander, and A. J. Miller,](https://doi.org/10.1175/JCLI-D-15-0789.1)
531 [2017: On the response of the Aleutian Low to greenhouse warming. *J. Climate*, 30,](https://doi.org/10.1175/JCLI-D-15-0789.1)
532 [3907-3925, doi: 10.1175/JCLI-D-15-0789.1](https://doi.org/10.1175/JCLI-D-15-0789.1)

533 Gu, D., & Philander, S. G. H. (1997). Interdecadal climate fluctuations that depend on
534 exchanges between the tropics and extratropics. *Science*, 275(5301), 805–807.
535 <https://doi.org/10.1126/science.275.5301.805>

536 Hu, D., & Guan, Z. (2018). Decadal relationship between the stratospheric arctic vortex and
537 pacific decadal oscillation. *Journal of Climate*, 31(9), 3371–3386.
538 <https://doi.org/10.1175/JCLI-D-17-0266.1>

539 Jin, F. F. (2001). Low-frequency modes of tropical ocean dynamics. *Journal of Climate*,
540 14(18), 3874–3881. [https://doi.org/10.1175/1520-](https://doi.org/10.1175/1520-0442(2001)014<3874:LFMOTO>2.0.CO;2)
541 [0442\(2001\)014<3874:LFMOTO>2.0.CO;2](https://doi.org/10.1175/1520-0442(2001)014<3874:LFMOTO>2.0.CO;2)
542 [0442\(2001\)014<3874:LFMOTO>2.0.CO;2](https://doi.org/10.1175/1520-0442(2001)014<3874:LFMOTO>2.0.CO;2)

543 [Joshi, M., Hall, R. A., Stevens, D. P., and Hawkins, E.: The modelled climatic response](https://doi.org/10.5194/esd-14-443-2023)
544 [to the 18.6-year lunar nodal cycle and its role in decadal temperature trends, *Earth*](https://doi.org/10.5194/esd-14-443-2023)
545 [Syst. Dynam.](https://doi.org/10.5194/esd-14-443-2023), 14, 443–455, <https://doi.org/10.5194/esd-14-443-2023>, 2023.

546 Joshi, M., Stringer, M., Van Der Wiel, K., O’Callaghan, A., & Fueglistaler, S. (2015).
547 IGCM4: A fast, parallel and flexible intermediate climate model. *Geoscientific Model*
548 *Development*, 8(4), 1157–1167. <https://doi.org/10.5194/gmd-8-1157-2015>
549 <https://doi.org/10.5194/gmd-8-1157-2015>

550 Klavans et al. (2023) Recent Atlantic multidecadal variability and its impacts are driven by
551 [external forcings-external forcings, submitted](#)
552 [, submitted](#)

553 Knight, J. R., Maidens, A., Watson, P. A. G., Andrews, M., Belcher, S., Brunet, G.,
554 Fereday, D., Folland, C. K., Scaife, A. A., & Slingo, J. (2017). Global meteorological
555 influences on the record UK rainfall of winter 2013-14. *Environmental Research*
556 *Letters*, 12(7). <https://doi.org/10.1088/1748-9326/aa693c>

557 Knutson, T. R., & Manabe, S. (1998). Model assessment of decadal variability and trends in
558 the tropical Pacific Ocean. In *Journal of Climate* (Vol. 11, Issue 9).
559 [https://doi.org/10.1175/1520-0442\(1998\)011<2273:MAODVA>2.0.CO;2](https://doi.org/10.1175/1520-0442(1998)011<2273:MAODVA>2.0.CO;2)
560 [https://doi.org/10.1175/1520-0442\(1998\)011<2273:MAODVA>2.0.CO;2](https://doi.org/10.1175/1520-0442(1998)011<2273:MAODVA>2.0.CO;2)

- 561 Kwon, Y. O., & Deser, C. (2007). North Pacific decadal variability in the community climate
562 system model version 2. *Journal of Climate*, 20(11), 2416–2433.
563 <https://doi.org/10.1175/JCLI4103.1>
- 564 Latif, M., & Barnett, T. P. (1996). Decadal climate variability over the North Pacific and
565 North America: Dynamics and predictability. *Journal of Climate*, 9(10), 2407–2423.
566 [https://doi.org/10.1175/1520-0442\(1996\)009<2407:DCVOTN>2.0.CO;2](https://doi.org/10.1175/1520-0442(1996)009<2407:DCVOTN>2.0.CO;2)
- 567 Liguori, G., & Di Lorenzo, E. (2019). Separating the North and South Pacific Meridional
568 Modes Contributions to ENSO and Tropical Decadal Variability. *Geophysical Research*
569 *Letters*, 46(2), 906–915. <https://doi.org/10.1029/2018GL080320>
- 570 Litzow, M. A., Malick, M. J., Bond, N. A., Cunningham, C. J., Gosselin, J. L., & Ward, E. J.
571 (2020). Quantifying a Novel Climate Through Changes in PDO-Climate and
572 ~~PDO-Salmon~~PDO-Salmon Relationships. *Geophysical Research Letters*, 47(16),
573 e2020GL087972. <https://doi.org/10.1029/2020GL087972>
- 574 Liu, Y., Sun, C., Kucharski, F., Li, J., Wang, C., & Ding, R. (2021). The North Pacific Blob
575 acts to increase the predictability of the Atlantic warm pool. *Environmental Research*
576 *Letters*, 16(6), 064034. <https://doi.org/10.1088/1748-9326/ac0030>
- 577 Lysne, J. A., Chang, P., & Giese, B. (1997). Impact of the extratropical Pacific on equatorial
578 variability. *Geophysical Research Letters*, 24(21), 2589–2592.
579 ~~<https://doi.org/10.1029/97GL02751>~~ <https://doi.org/10.1029/97GL02751>
- 580 ~~[Mantua, N. J., Hare, S. R., Zhang, Y., Wallace, J. M., & Francis, R. C. \(1997\). A Pacific](#)~~
581 ~~[Interdecadal Climate Oscillation with Impacts on Salmon Production. *Bulletin of the*](#)~~
582 ~~[American Meteorological Society](#), 78(6), 1069–1079. [https://doi.org/10.1175/1520-](https://doi.org/10.1175/1520-0477(1997)078<1069:APICOW>2.0.CO;2)~~
583 ~~[0477\(1997\)078<1069:APICOW>2.0.CO;2](#)~~
- 584 Mahajan, S., Saravanan, R., & Chang, P. (2009). The role of the wind-evaporation-sea
585 surface temperature (WES) feedback in air-sea coupled tropical variability.
586 ~~[Atmospheric Research](#), 94(1), 19–36. <https://doi.org/10.1016/j.atmosres.2008.09.017>~~
- 587 ~~[Atmospheric Research](#), 94(1), 19–36. <https://doi.org/10.1016/j.atmosres.2008.09.017>~~
- 588 Martin, Z., Orbe, C., Wang, S., & Sobel, A. (2021). The MJO–QBO relationship in a

589 GCM with stratospheric nudging. *Journal of Climate*, 34(11), 4603–4624.
590 <https://doi.org/10.1175/JCLI-D-20-0636.1>

591 McCreary, J. P., & Peng Lu. (1994). Interaction between the subtropical and equatorial
592 ocean circulations: the subtropical cell. *Journal of Physical Oceanography*, 24(2), ~~466–~~
593 ~~497~~. [https://doi.org/10.1175/1520-0485\(1994\)024<0466:IBTSAE>2.0.CO;2](https://doi.org/10.1175/1520-0485(1994)024<0466:IBTSAE>2.0.CO;2)
594 ~~466–497~~. [https://doi.org/10.1175/1520-0485\(1994\)024<0466:IBTSAE>2.0.CO;2](https://doi.org/10.1175/1520-0485(1994)024<0466:IBTSAE>2.0.CO;2)

595 Nagano, A., & Wakita, M. (2019). Wind-driven decadal sea surface height and main
596 pycnocline depth changes in the western subarctic North Pacific. *Progress in Earth*
597 *and Planetary Science*, 6(1), 1–26. <https://doi.org/10.1186/s40645-019-0303-0>

598 Newman, M., Alexander, M. A., Ault, T. R., Cobb, K. M., Deser, C., Di Lorenzo, E., Mantua,
599 N. J., Miller, A. J., Minobe, S., Nakamura, H., Schneider, N., Vimont, D. J., Phillips, A.
600 ~~S., Scott, J. D., & Smith, C. A. (2016). The Pacific decadal oscillation, revisited. *Journal*~~
601 ~~of Climate~~, 29(12), 4399–4427. <https://doi.org/10.1175/JCLI-D-15-0508.1>
602 ~~S., Scott, J. D., & Smith, C. A. (2016). The Pacific decadal oscillation, revisited.~~
603 ~~*Journal of Climate*, 29(12), 4399–4427. https://doi.org/10.1175/JCLI-D-15-0508.1~~

604 Pickart, R. S., Moore, G. W. K., Macdonald, A. M., Renfrew, I. A., Walsh, J. E., & Kessler,
605 W. S. (2009). Seasonal evolution of Aleutian low pressure systems: Implications for the
606 North Pacific subpolar circulation. *Journal of Physical Oceanography*, 39(6), ~~1317–~~
607 ~~1339~~. <https://doi.org/10.1175/2008JPO3891.1>
608 ~~1317–1339~~. <https://doi.org/10.1175/2008JPO3891.1>

609 Pierce, D. W., Barnett, T. P., & Latif, M. (2000). Connections between the Pacific Ocean
610 Tropics and midlatitudes on decadal timescales. *Journal of Climate*, 13(6), 1173–
611 1194. [https://doi.org/10.1175/1520-0442\(2000\)013<1173:CBTPOT>2.0.CO;2](https://doi.org/10.1175/1520-0442(2000)013<1173:CBTPOT>2.0.CO;2)

612 Richter, J. H., Deser, C., & Sun, L. (2015). Effects of stratospheric variability on El Niño.
613 *Environmental Research Letters*, 10(12). [https://doi.org/10.1088/174893261748-](https://doi.org/10.1088/174893261748-9326/10/12/124021)
614 ~~9326/10/12/124021~~

615 Schneider, N., & Cornuelle, B. D. (2005). The forcing of the Pacific Decadal Oscillation.

- 616 *Journal of Climate*, 18(21), 4355–4373. <https://doi.org/10.1175/JCLI3527.1>
- 617 Schneider, N., Miller, A. J., & Pierce, D. W. (2002). Anatomy of North Pacific decadal
618 variability. In *Journal of Climate* (Vol. 15, Issue 6). [https://doi.org/10.1175/1520-
619 0442\(2002\)015<0586:AONPDV>2.0.CO;2](https://doi.org/10.1175/1520-0442(2002)015<0586:AONPDV>2.0.CO;2)
- 620 ~~[0442\(2002\)015<0586:AONPDV>2.0.CO;2](https://doi.org/10.1175/1520-0442(2002)015<0586:AONPDV>2.0.CO;2)~~
- 621 Simon, A., Gastineau, G., Frankignoul, C., Rousset, C., & Codron, F. (2021). Transient
622 climate response to Arctic Sea ice loss with two ice-constraining methods. *Journal of
623 Climate*, 34(9), 3295–3310. <https://doi.org/10.1175/JCLI-D-20-0288.1>
- 624 Smith, D. M., Booth, B. B. B., Dunstone, N. J., Eade, R., Hermanson, L., Jones, G. S.,
625 Scaife, A. A., Sheen, K. L., & Thompson, V. (2016). Role of volcanic and
626 anthropogenic aerosols in the recent global surface warming slowdown. *Nature
627 Climate Change*, 6(10), 936–940. <https://doi.org/10.1038/nclimate3058>
- 628 Sugimoto, S., & Hanawa, K. (2009). Decadal and interdecadal variations of the Aleutian
629 Low activity and their relation to upper oceanic variations over the North Pacific.
630 ~~*Journal of the Meteorological Society of Japan*, 87(4), 601–614.~~
631 ~~<https://doi.org/10.2151/jmsj.87.601>~~
- 632 ~~*Journal of the Meteorological Society of Japan*, 87(4), 601–614.~~
633 ~~<https://doi.org/10.2151/jmsj.87.601>~~
- 634 Sun, J., & Wang, H. (2006). Relationship between Arctic Oscillation and Pacific Decadal
635 Oscillation on decadal timescale. *Chinese Science Bulletin*, 51(1), 75–79.
636 <https://doi.org/10.1007/s11434-004-0221-3>
- 637 Sun, T., & Okumura, Y. M. (2019). Role of stochastic atmospheric forcing from the south
638 and North Pacific in tropical Pacific decadal variability. *Journal of Climate*, 32(13),
639 ~~[4013–4038. https://doi.org/10.1175/JCLI-D-18-0536.1](https://doi.org/10.1175/JCLI-D-18-0536.1)~~
- 640 ~~[4013–4038. https://doi.org/10.1175/JCLI-D-18-0536.1](https://doi.org/10.1175/JCLI-D-18-0536.1)~~
- 641 Taguchi, B., Xie, S. P., Schneider, N., Nonaka, M., Sasaki, H., & Sasai, Y. (2007). Decadal
642 variability of the Kuroshio Extension: Observations and an eddy-resolving model
643 hindcast. *Journal of Climate*, 20(11), 2357–2377. <https://doi.org/10.1175/JCLI4142.1>

- 644 Trenberth, K. E., & Hurrell, J. W. (1994). Decadal atmosphere-ocean variations in the
645 Pacific. *Climate Dynamics*, 9(6), 303–319. <https://doi.org/10.1007/BF00204745>
- 646 Vimont, D. J. (2005). The contribution of the interannual ENSO cycle to the spatial pattern
647 of decadal ENSO-like variability. In *Journal of Climate* (Vol. 18, Issue 12).
648 <https://doi.org/10.1175/JCLI3365.1>
- 649 Vimont, D. J., Battisti, D. S., & Hirst, A. C. (2001). Footprinting: A seasonal connection
650 between the tropics and mid-latitudes. *Geophysical Research Letters*, 28(20), 3923–
651 [3926. https://doi.org/10.1029/2001GL013435](https://doi.org/10.1029/2001GL013435)
652 ~~[3926. https://doi.org/10.1029/2001GL013435](https://doi.org/10.1029/2001GL013435)~~
- 653 Vimont, D. J., Battisti, D. S., & Hirst, A. C. (2002). Pacific interannual and interdecadal
654 equatorial variability in a 1000-Yr simulation of the CSIRO coupled general circulation
655 model. *Journal of Climate*, 15(2), 160–178. [https://doi.org/10.1175/1520-
656 \[0442\\(2002\\)015<0160:PIAIEV>2.0.CO;2\]\(https://doi.org/10.1175/1520-0442\(2002\)015<0160:PIAIEV>2.0.CO;2\)
657 ~~\[0442\\(2002\\)015<0160:PIAIEV>2.0.CO;2\]\(https://doi.org/10.1175/1520-0442\(2002\)015<0160:PIAIEV>2.0.CO;2\)~~](https://doi.org/10.1175/1520-0442(2002)015<0160:PIAIEV>2.0.CO;2)
- 658 Vimont, D. J., Wallace, J. M., & Battisti, D. S. (2003). The seasonal footprinting mechanism
659 in the Pacific: Implications for ENSO. *Journal of Climate*, 16(16), 2668–2675.
660 [https://doi.org/10.1175/1520-0442\(2003\)016<2668:TSMIT>2.0.CO;2](https://doi.org/10.1175/1520-0442(2003)016<2668:TSMIT>2.0.CO;2)
- 661 Wang, H., Kumar, A., Wang, W., & Xue, Y. (2012). Seasonality of the Pacific decadal
662 oscillation. *Journal of Climate*, 25(1), 25–38. <https://doi.org/10.1175/2011JCLI4092.1>
- 663 Watson, P. A. G., Weisheimer, A., Knight, J. R., & Palmer, T. N. (2016). The role of the
664 tropical West Pacific in the extreme Northern Hemisphere winter of 2013/2014. *Journal
665 of Geophysical Research*, 121(4), 1698–1714. <https://doi.org/10.1002/2015JD024048>
666 ~~[Journal of Geophysical Research, 121\(4\), 1698–1714.](https://doi.org/10.1002/2015JD024048)~~
667 ~~<https://doi.org/10.1002/2015JD024048>~~
- 668 Webb, D. J. (1996). An ocean model code for array processor computers. *Computers and
669 Geosciences*, 22(5), 569–578. [https://doi.org/10.1016/0098-3004\(95\)00133-6](https://doi.org/10.1016/0098-3004(95)00133-6)

670 Wills, R. C. J., Battisti, D. S., Proistosescu, C., Thompson, L. A., Hartmann, D. L., &
671 Armour, K. C. (2019). Ocean Circulation Signatures of North Pacific Decadal
672 Variability. *Geophysical Research Letters*, *46*(3), 1690–1701.
673 <https://doi.org/10.1029/2018GL080716>

674 Xie, S. P., & Tanimoto, Y. (1998). A pan-Atlantic decadal climate oscillation. *Geophysical*
675 *Research Letters*, *25*(12), 2185–2188. <https://doi.org/10.1029/98GL01525>

676 Zhang, D., & McPhaden, M. J. (2006). Decadal variability of the shallow Pacific meridional
677 overturning circulation: Relation to tropical sea surface temperatures in observations
678 and climate change models. *Ocean Modelling*, *15*(3–4), 250–273.
679 <https://doi.org/10.1016/j.ocemod.2005.12.005>

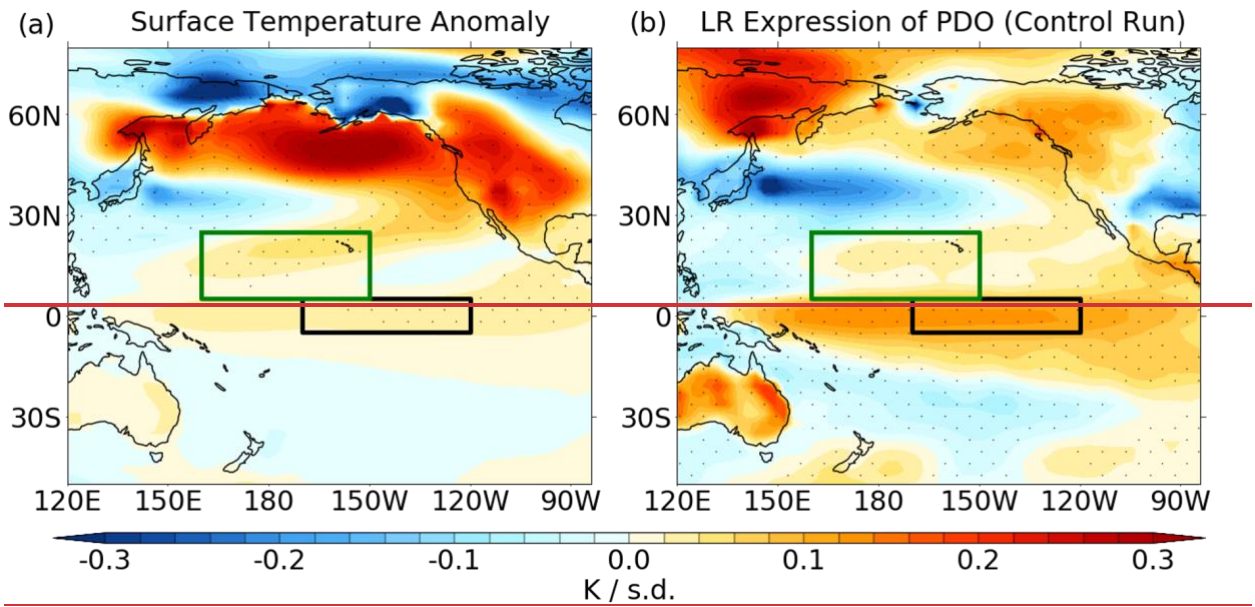
680 Zhang, Y., Xie, S. P., Kosaka, Y., & Yang, J. C. (2018). Pacific decadal oscillation: Tropical
681 Pacific forcing versus internal variability. *Journal of Climate*, *31*(20), 8265–8279.
682 <https://doi.org/10.1175/JCLI-D-18-0164.1>
683 ~~<https://doi.org/10.1175/JCLI-D-18-0164.1>~~

684 Zhao, Y., Newman, M., Capotondi, A., Lorenzo, E. Di, & Sun, D. (2021). Removing the
685 effects of tropical dynamics from north pacific climate variability. *Journal of Climate*,
686 *34*(23), 9249–9265. <https://doi.org/10.1175/JCLI-D-21-0344.1>

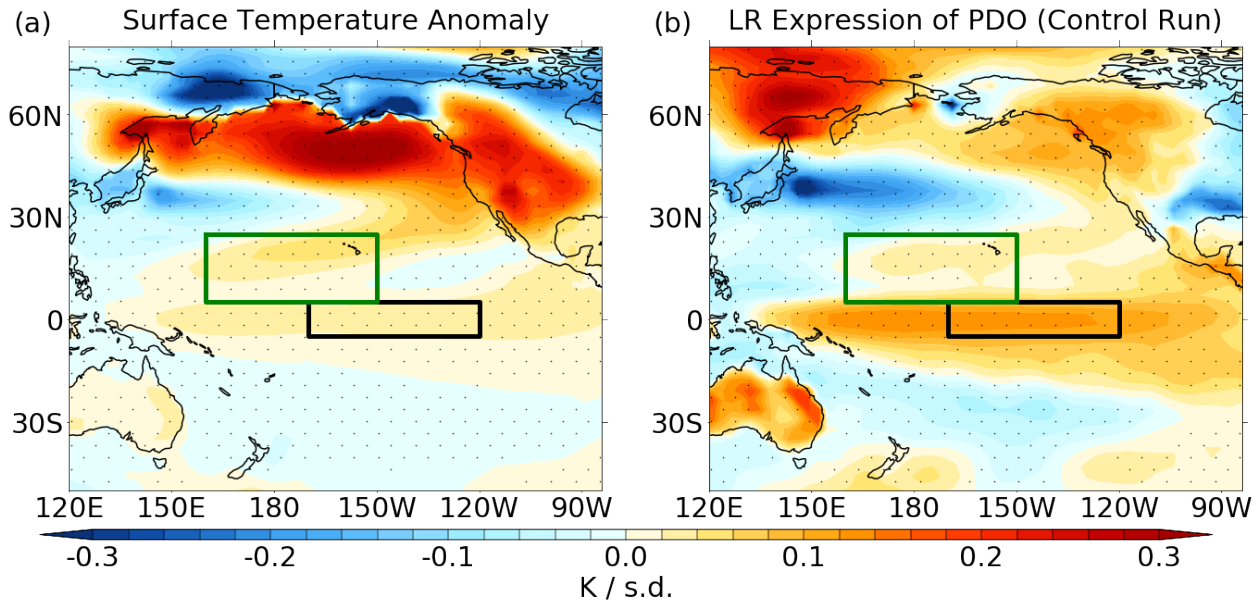
687
688
689
690
691
692
693
694
695
696
697
698
699

700
701
702
703
704
705
706
707
708
709
710
711
712
713
714

Figures



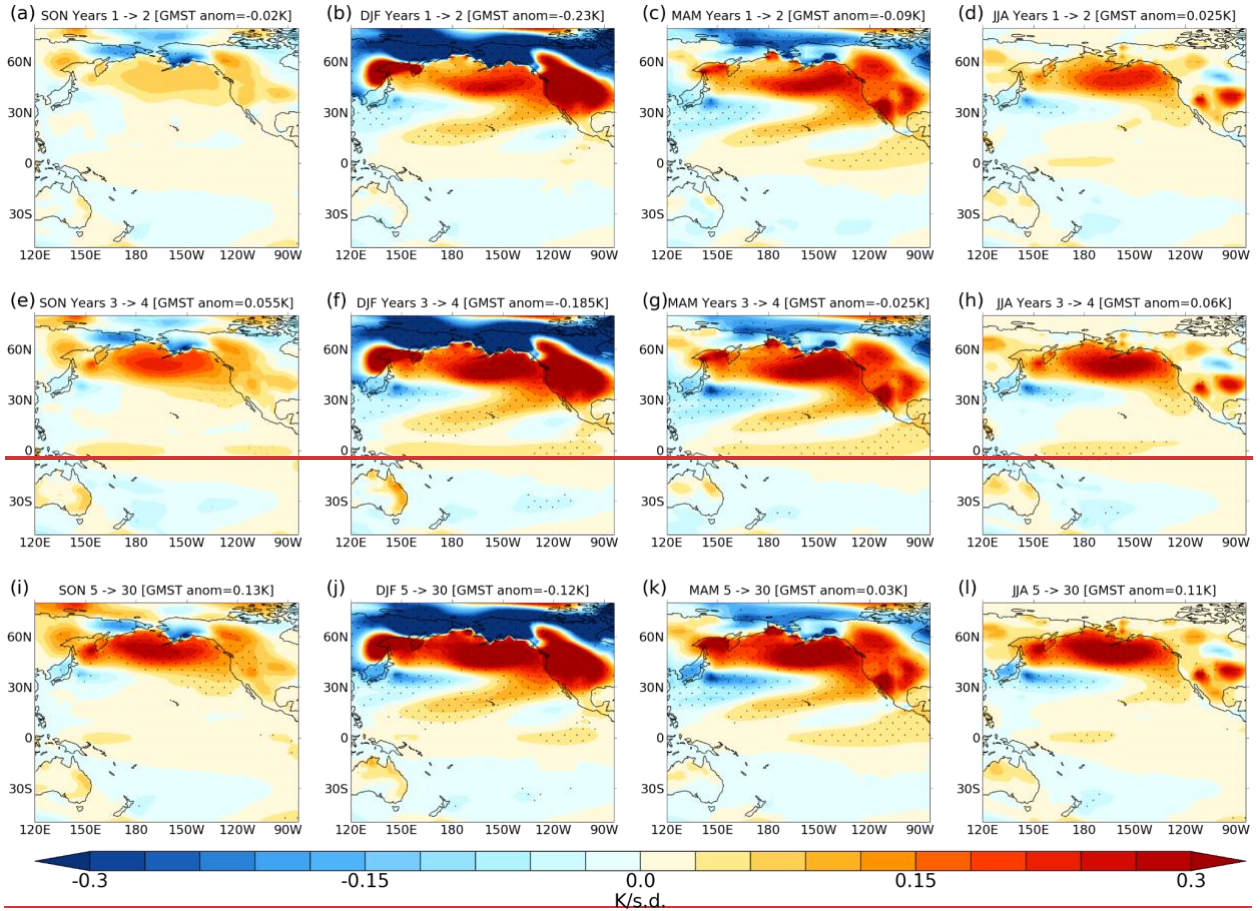
715
716
717
718
719



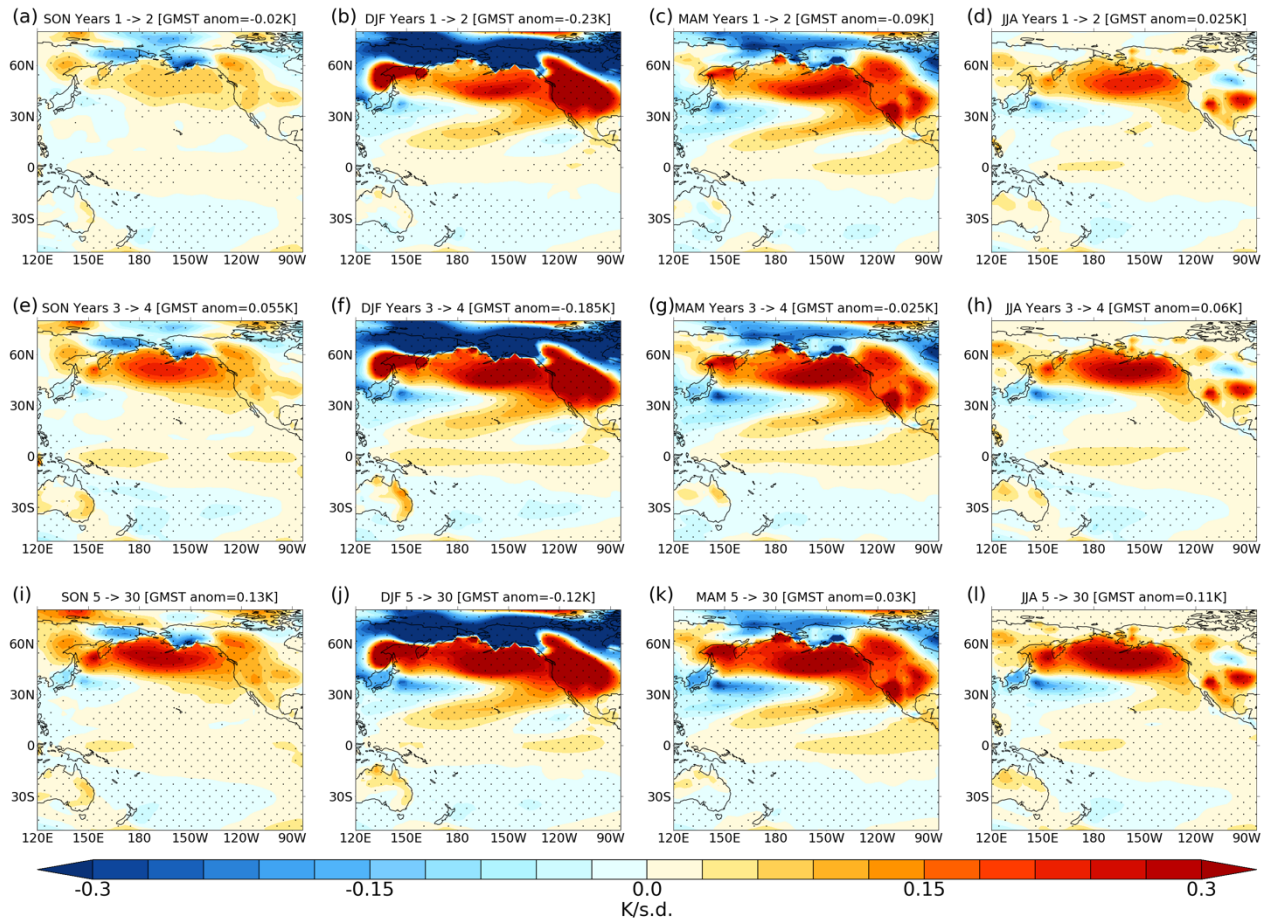
720

721 **Figure 1:** Annual mean surface temperature anomalies for (a) regression onto the PDO
 722 index in CONTROL; (b) ensemble mean anomaly in NUDGED averaged over years 1-30;
 723 (b) linear regression (LR) onto the PDO index in CONTROL. The anomaly between
 724 NUDGED and CONTROL is projected onto the first EOF from the control run to generate
 725 a pseudo-PC. The anomaly is divided by the pseudo-PC to calculate the anomaly per
 726 standard deviation of the PDO index, expressed in a similar way to that derived from
 727 CONTROL. Units are K per standard deviation. Stippling denotes anomalies that are
 728 significant at the 95% level. Green and black boxes show the regions for the mixed layer
 729 heat budget analysis.

730



731
732
733



734

735

736

737

738

739

740

741

742

743

744

745

746

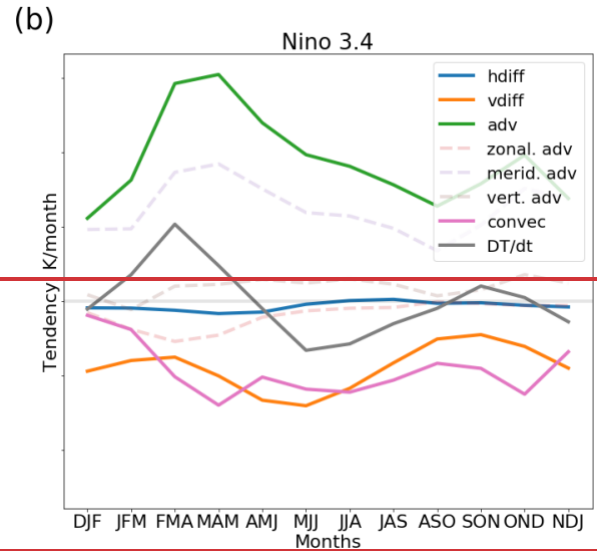
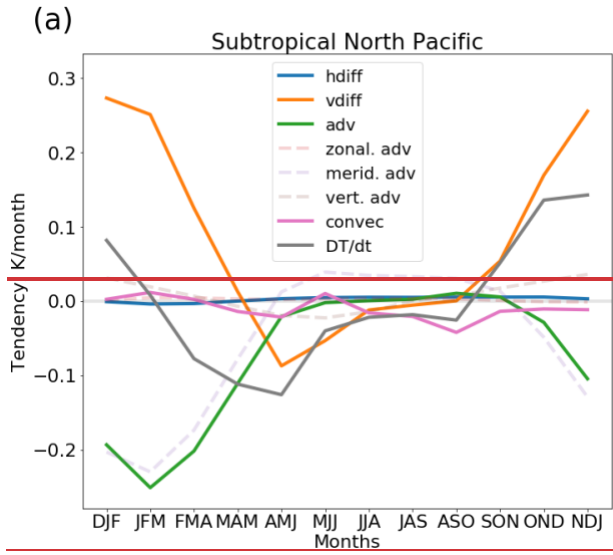
747

748

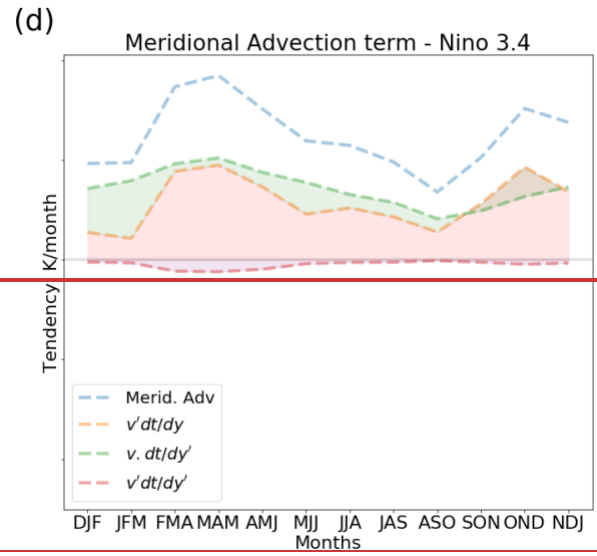
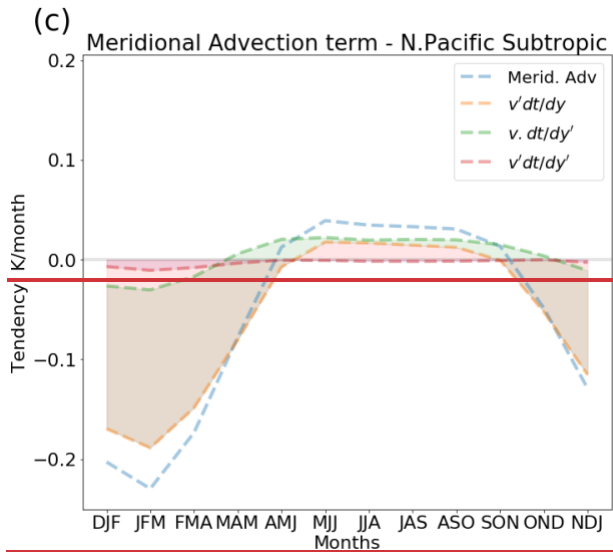
749

Figure 2: Seasonal mean surface temperature anomalies in NUDGED expressed per unit PDO index $[K/\sigma]$ for SON, DJF, MAM and JJA. AnomaliesComposite anomalies are shown for years 1-2 (a-d), years 3-4 (e-h) and years 5-30 (i-l). Global mean surface temperature anomalies are shown in the header. Stippling denotes anomalies that are significant at the 95% level.

750
751

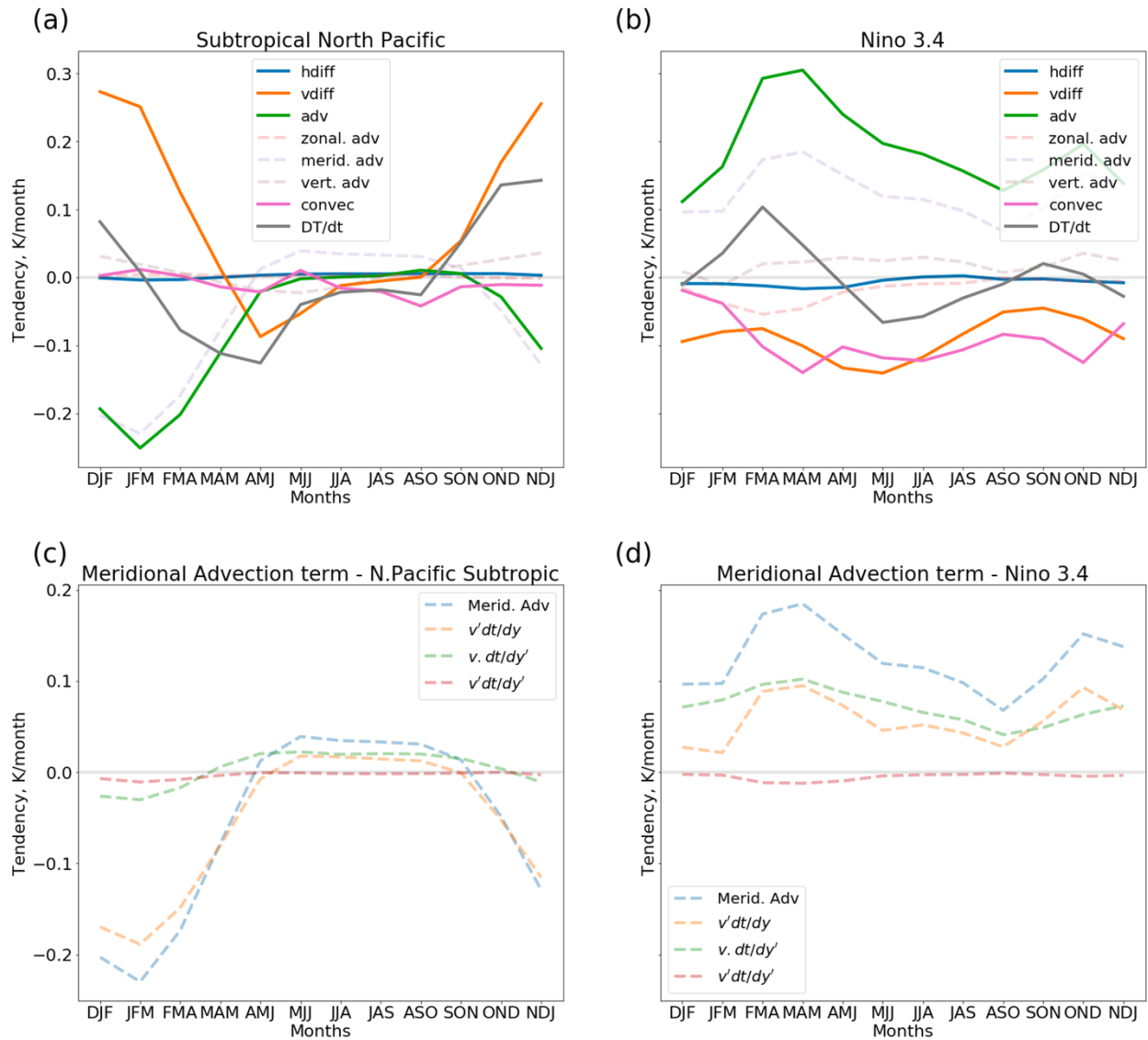


752
753
754



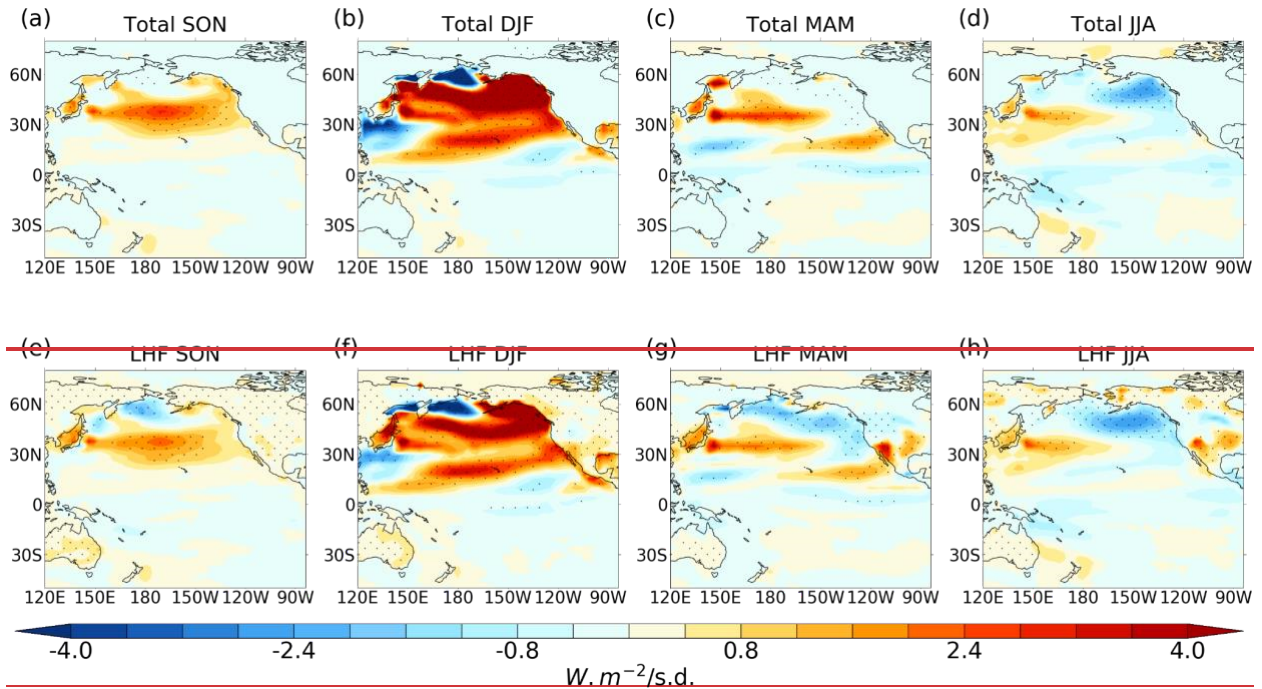
755
756
757
758
759
760
761
762
763

764
765



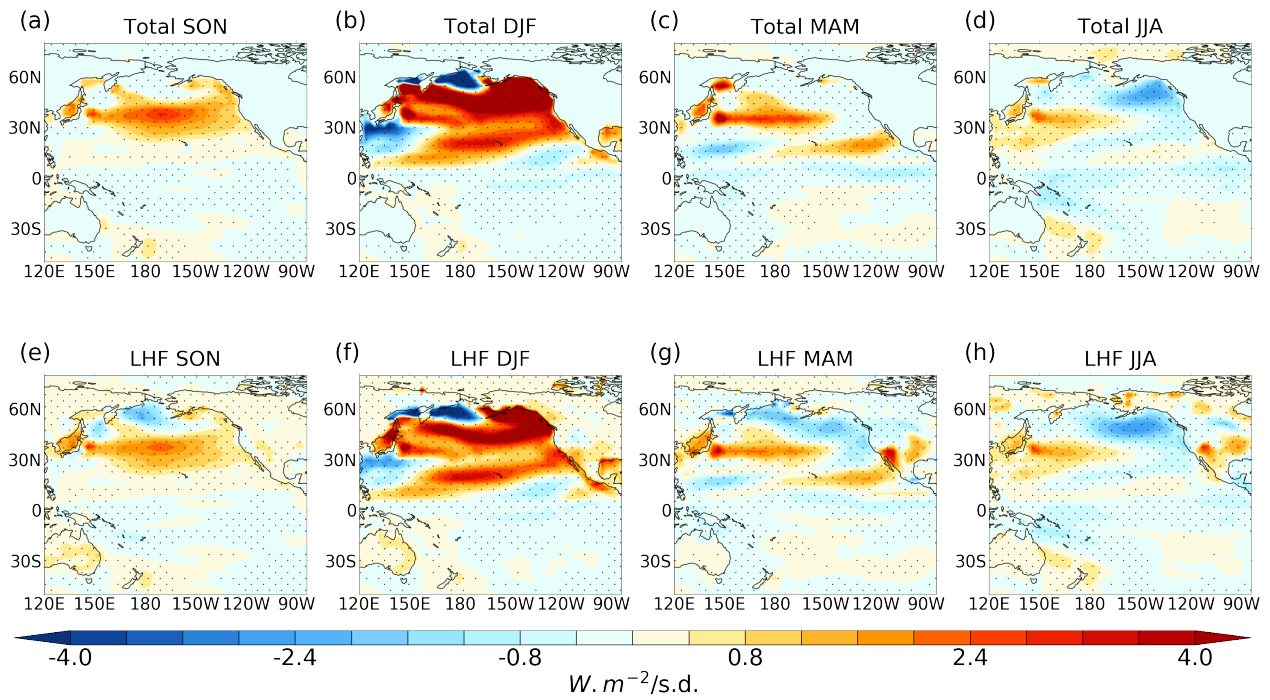
766
767

768 **Figure 3:** Years 1-30, 3-month moving average of **anomalous NUDGED minus CONTROL**
769 mixed layer temperature tendencies and constituent heat budget terms for the (a)
770 subtropical North Pacific and (b) Niño 3.4 regions. (c,d) show the meridional advection
771 term and its linear expansion. -The subtropical North Pacific and Niño 3.4 domains are
772 indicated by the boxes in Fig. 1.



773

774



775

776

777 **Figure 4:** (a-d) SeasonalYears 1-30 seasonal mean net surface heat flux anomalies in
 778 NUDGED. (e-h):

779 SeasonalYears 1-30 seasonal mean latent heat flux anomaly in NUDGED. Positive
 780 denotes downward flux.

781 Stippling denotes anomalies that are statistically significant at the 95% level. Units: $\text{W m}^2\text{m}^{-2}$ per standard deviation.
782

783

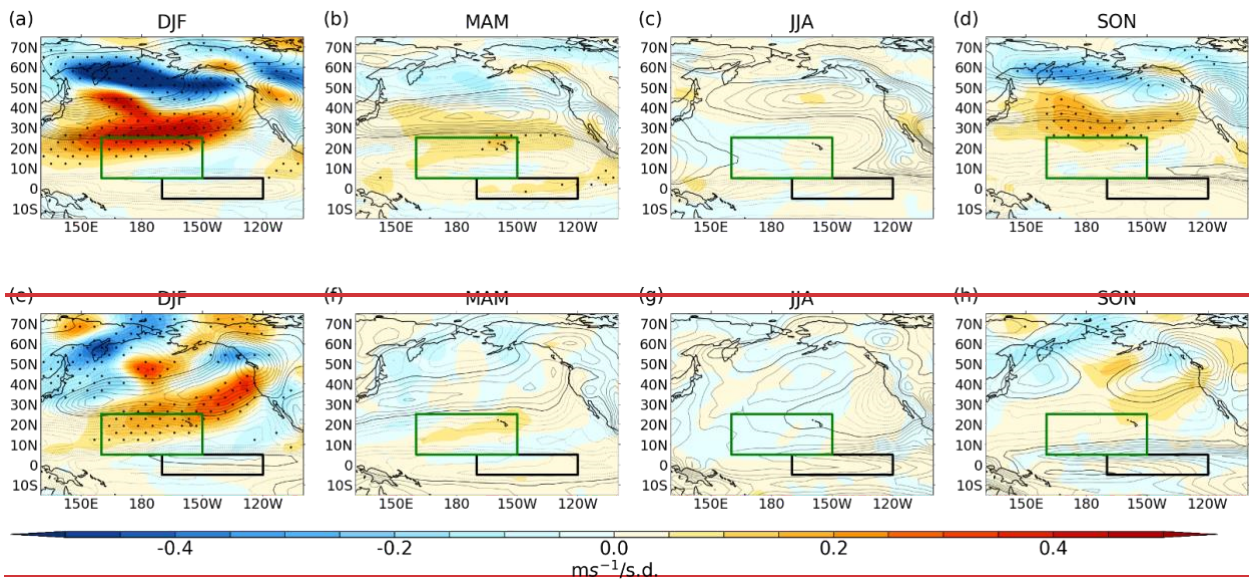
784

785

786

787

788



789

790

791

792

793

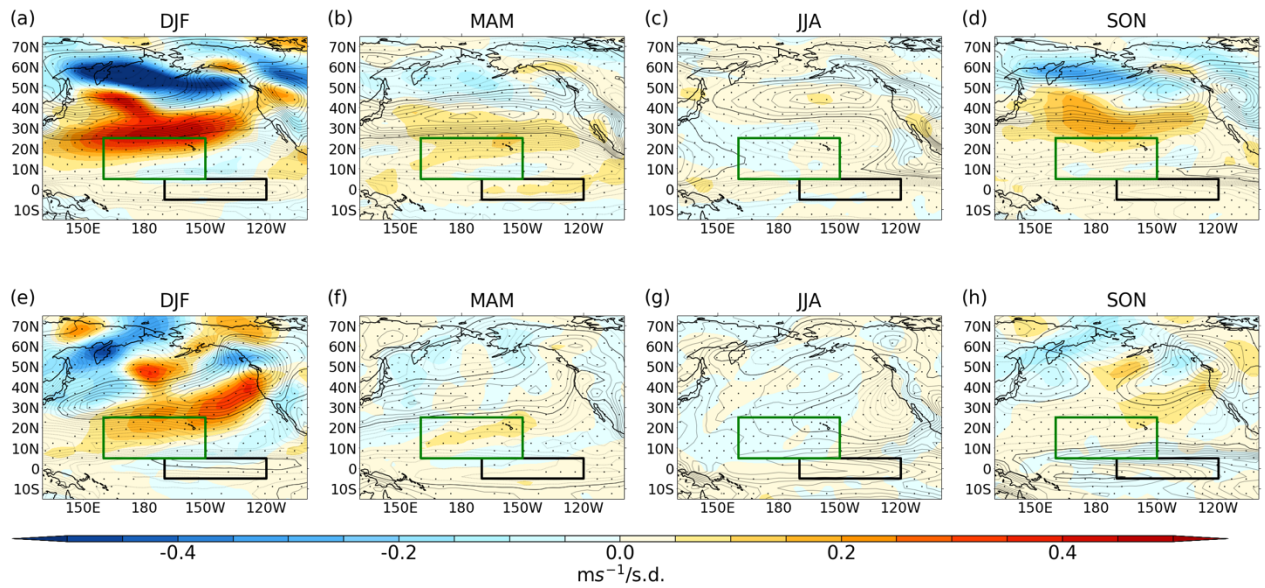
794

795

796

797

798



799

800 **Figure 5:** ~~Seasonal~~Years 1-30 seasonal mean NUDGED-CONTROL near-surface
 801 (lowest model level) wind anomalies for (a-d) zonal and (e-
 802 h) meridional wind. Contours show climatology of CONTROL (dashed lines are negative
 803 values, contour interval 1 m s⁻¹). Stippling denotes anomalies that are significant at the
 804 95% level.

805

806

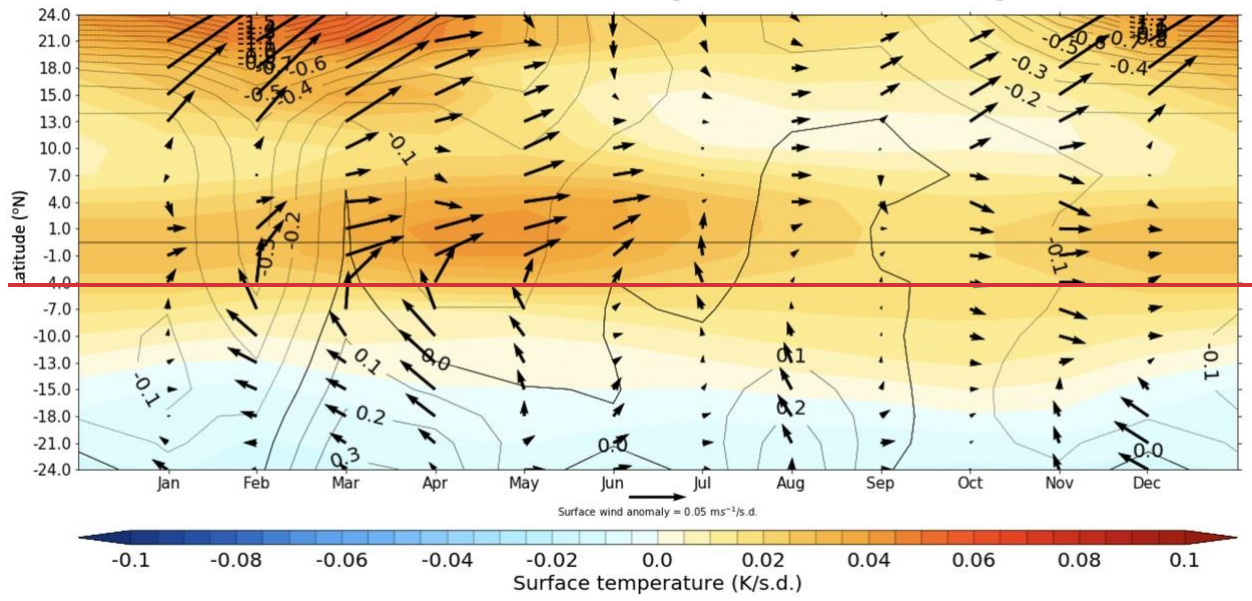
807

808

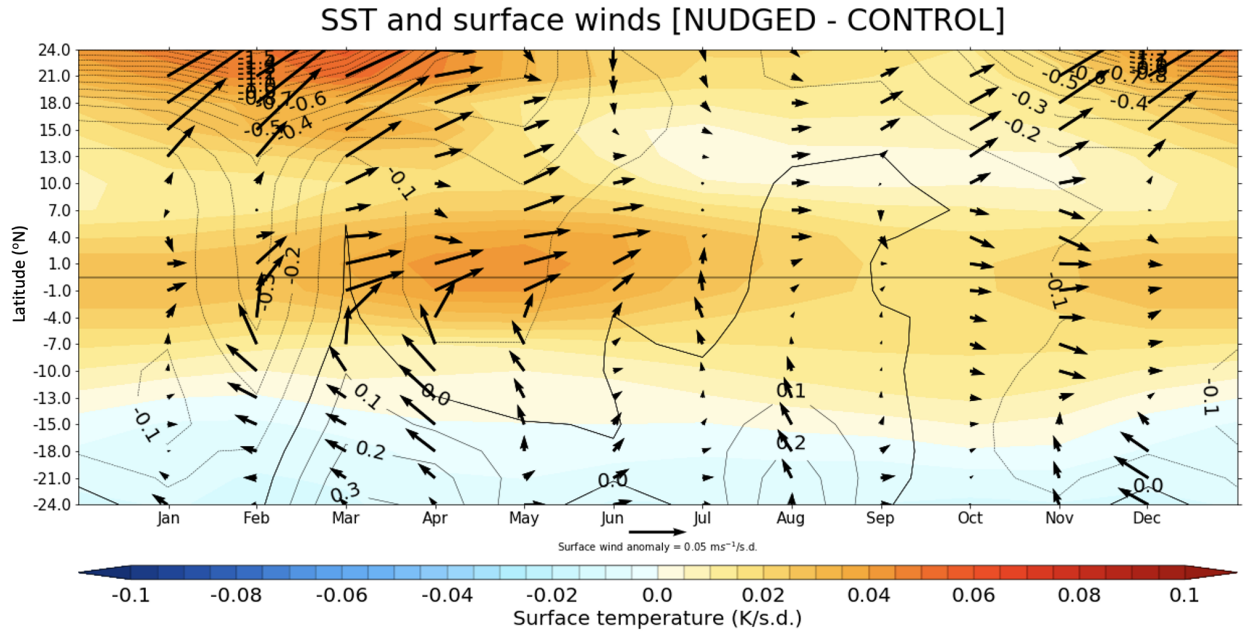
809

810

SST and surface winds [NUDGED - CONTROL]



811
812
813
814
815
816
817
818



819

820

821

822

823

824

825

826

827

828

829

830

831

832

833

834

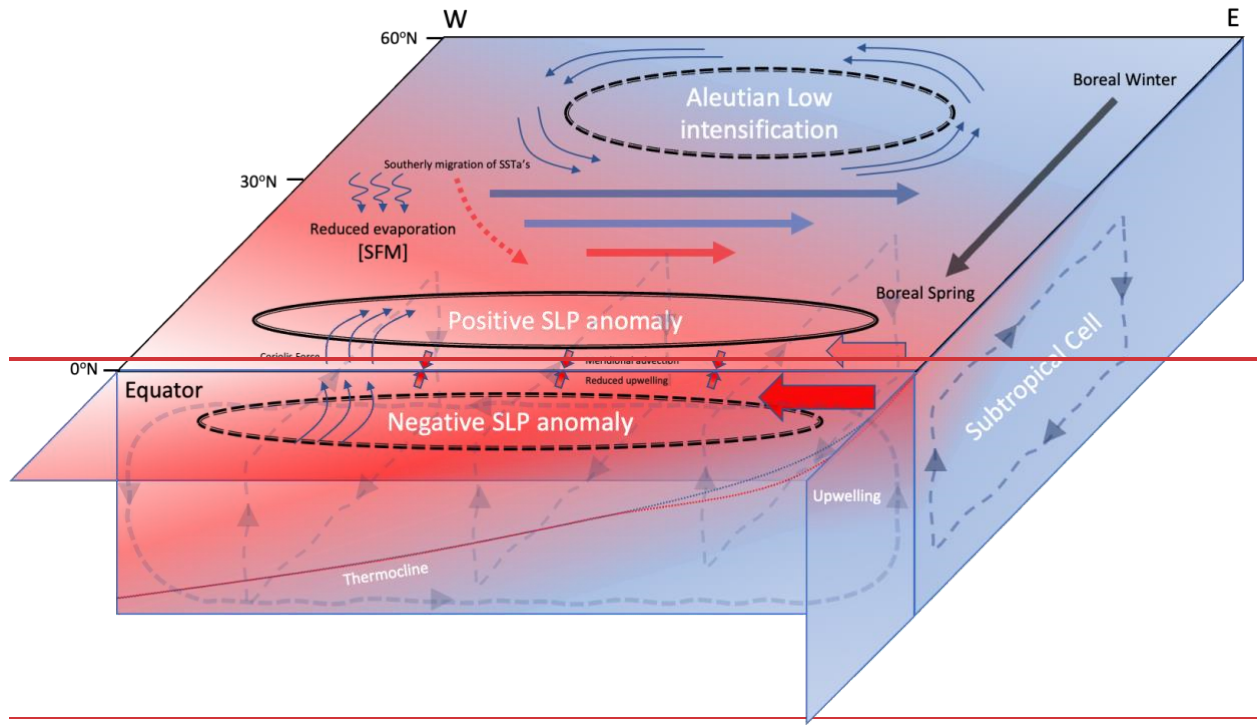
835

836

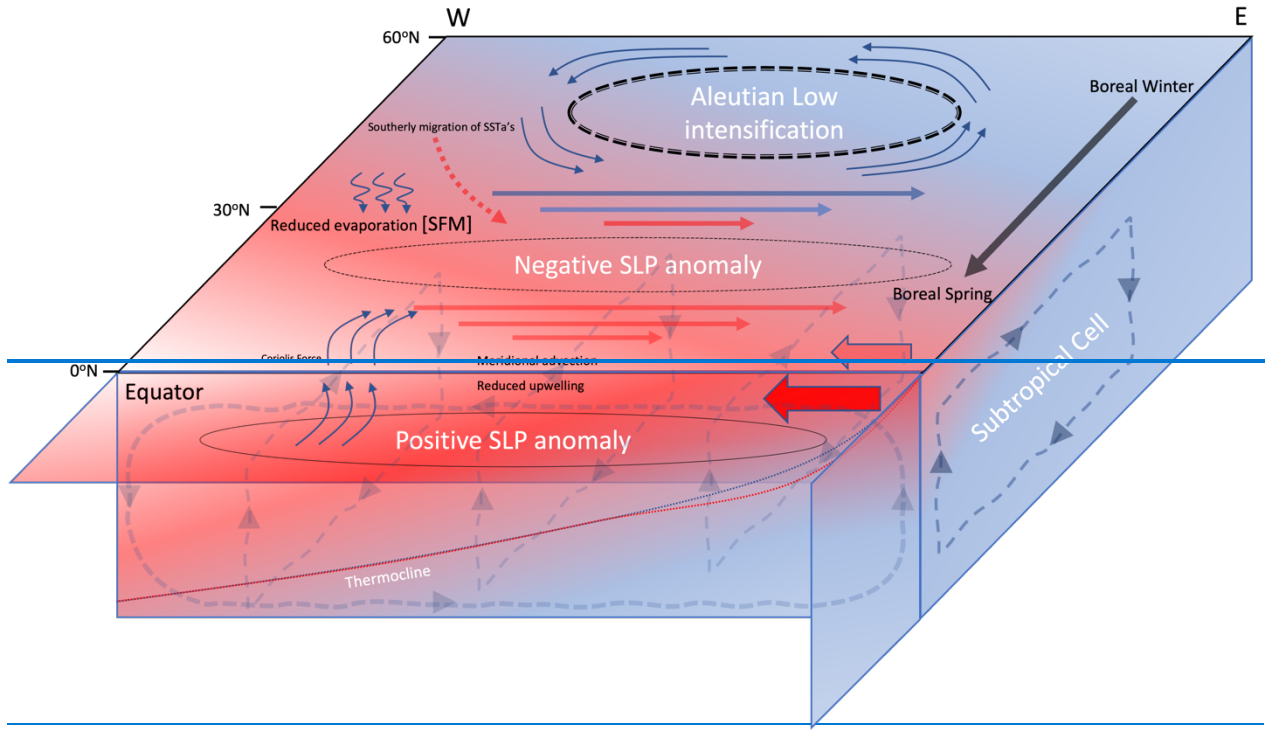
837

838

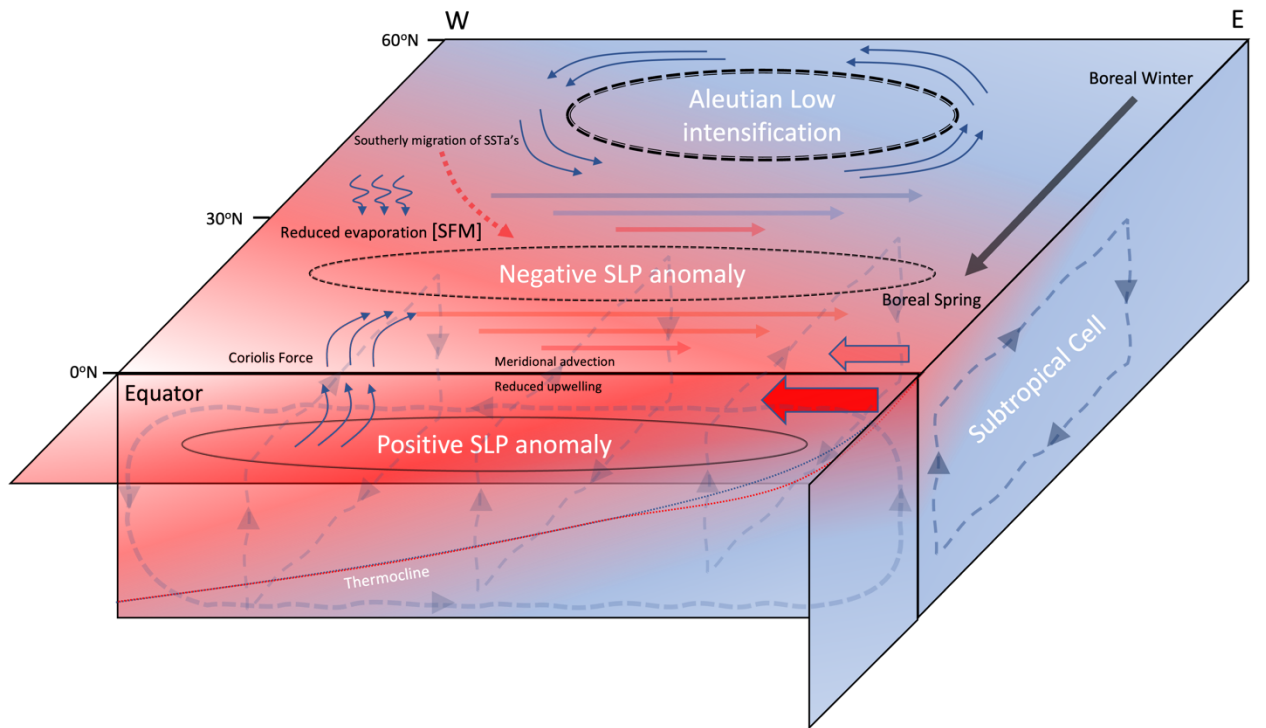
Figure 6: LatitudeYears 1-30 latitude-time section of NUDGED minus CONTROL SST anomaly (K/ σ : shading), surface pressure (hPa/ σ : contours) and near-surface wind anomaly (m s^{-1} / σ : vectors) averaged over the centraleasterncentral-eastern tropical Pacific (205°W-80°W).



839
 840
 841
 842
 843
 844
 845
 846
 847



848



849

850 **Figure 7:** Schematic depicting the mechanisms involved in the tropical SST anomalies
 851 manifest as a result from an intensification of the AL. An intensified AL (dashed black
 852 line) imposed during boreal winter is associated with intensified westerlies (reduced

853 easterlies; solid arrows) in the ~~extra-tropics~~subtropics and downward latent heat transfer.
854 The migration of the SST anomalies southward during boreal winter is associated with
855 westerly anomalies in the subtropics (reduced trades)~~a southerly shift in the westerly~~
856 anomalies. The westerly anomalies act to weaken the background trades (filled red
857 arrows) which reduces latent heating cooling due to decreased evaporation and hence
858 an increase in ~~extra-tropical~~subtropical Pacific SSTs. In the season after nudging, the
859 temperature asymmetry ~~either side of~~about the equator induces an SLP gradient (solid
860 line – positive SLP; dashed line – negative SLP) that drives southerly winds across the
861 equator. The Coriolis force acts to turn the southerly winds in the southern hemisphere
862 westward and in the northern hemisphere eastward. When these anomalous winds are
863 imposed on the background easterly trade winds (filled red arrows), the southerlies
864 south of the equator increase the wind speed and therefore evaporative cooling, whilst
865 north of the equator the background trades are weakened, reducing evaporative cooling.
866 The westerly wind anomalies along the equator ~~The changes to the wind driven surface~~
867 ~~state act to~~ deepen the thermocline in the eastern tropical Pacific (red dotted line) and
868 reduce upwelling/divergence of cooler waters at the equator.

869 _____
870 _____
871 _____
872 647 _____
873 _____
874 _____
875 _____